AGU PUBLICATIONS

Paleoceanography

RESEARCH ARTICLE
10.1002/2017PA003135

Key Points:
- Distinct neodymium water mass signature recorded in intermediate/deep waters in the SW Pacific during the Eocene
- Local deep water formation on Adélie Coast during Eocene greenhouse warmth
- A previously unidentified Antarctic erosional event occurred at 49-48 Ma

Supporting Information:
- Supporting Information S1

Correspondence to:
C. E. Huck,
c.e.huck@soton.ac.uk

Citation:
Huck, C. E., T. van de Flierdt, S. M. Bohaty, and S. J. Hammond (2017), Antarctic climate, Southern Ocean circulation patterns, and deep water formation during the Eocene, *Paleoceanography*, *32*, doi:10.1002/2017PA003135.

Received 10 APR 2017
Accepted 29 MAY 2017
Accepted article online 11 JUN 2017

Antarctic climate, Southern Ocean circulation patterns, and deep water formation during the Eocene

Claire E. Huck[1,2], Tina van de Flierdt[1], Steven M. Bohaty[2], and Samantha J. Hammond[3]

[1]Department of Earth Science and Engineering, Imperial College London, London, UK, [2]Ocean and Earth Science, National Oceanography Centre Southampton, University of Southampton, Southampton, UK, [3]Environment, Earth and Ecosystems Department, Open University, Milton Keynes, UK

Abstract We assess early-to-middle Eocene seawater neodymium (Nd) isotope records from seven Southern Ocean deep-sea drill sites to evaluate the role of Southern Ocean circulation in long-term Cenozoic climate change. Our study sites are strategically located on either side of the Tasman Gateway and are positioned at a range of shallow (<500 m) to intermediate/deep (~1000–2500 m) paleowater depths. Unradiogenic seawater Nd isotopic compositions, reconstructed from fish teeth at intermediate/deep Indian Ocean pelagic sites (Ocean Drilling Program (ODP) Sites 738 and 757 and Deep Sea Drilling Project (DSDP) Site 264), indicate a dominant Southern Ocean-sourced contribution to regional deep waters ($\varepsilon_{Nd(t)} = -9.3 \pm 1.5$). IODP Site U1356 off the coast of Adélie Land, a locus of modern-day Antarctic Bottom Water production, is identified as a site of persistent deep water formation from the early Eocene to the Oligocene. East of the Tasman Gateway an additional local source of intermediate/deep water formation is inferred at ODP Site 277 in the SW Pacific Ocean ($\varepsilon_{Nd(t)} = -8.7 \pm 1.5$). Antarctic-proximal shelf sites (ODP Site 1171 and Site U1356) reveal a pronounced erosional event between 49 and 48 Ma, manifested by ~2 ε_{Nd} unit negative excursions in seawater chemistry toward the composition of bulk sediments at these sites. This erosional event coincides with the termination of peak global warmth following the Early Eocene Climatic Optimum and is associated with documented cooling across the study region and increased export of Antarctic deep waters, highlighting the complexity and importance of Southern Ocean circulation in the greenhouse climate of the Eocene.

1. Introduction

The Paleogene time period (66 to 23 Ma) encompasses the transition from the warm "greenhouse" climate state of the late Paleocene and early Eocene (59 to 48 Ma) to the colder "icehouse" climate state of the Oligocene (34 to 23 Ma) [*Zachos et al.*, 2008]. The warmest climatic conditions of the Paleogene occurred during the Early Eocene Climatic Optimum (EECO) (~52 to 48 Ma) [*Sexton et al.*, 2011; *Zachos et al.*, 2008] when deep ocean temperatures reached ~12°C [*Littler et al.*, 2014; *Zachos et al.*, 2001] and polar regions were characterized by extreme warmth with Antarctic coastal summer temperatures in excess of 20°C [*Pross et al.*, 2012]. Following the EECO, global temperatures declined until the prevailing greenhouse conditions ended at the Eocene-Oligocene Transition (EOT) (~34 Ma) with continental-scale glaciation of Antarctica and ocean cooling [e.g., *Coxall et al.*, 2005; *Dunkley Jones et al.*, 2008; *Ehrmann et al.*, 1992; *Houben et al.*, 2013; *Lear et al.*, 2008; *Liu et al.*, 2009; *Passchier et al.*, 2017; *Zachos et al.*, 2001].

The relative role of decreasing atmospheric CO_2 versus changing Southern Ocean circulation patterns resulting from the opening of high-latitude ocean gateways (i.e., Drake Passage and Tasman Gateway) in the transition from greenhouse to icehouse climates during the Paleogene has been much debated [e.g., *DeConto and Pollard*, 2003; *Galeotti et al.*, 2016; *Goldner et al.*, 2014; *Huber and Nof*, 2006; *Kennett*, 1977; *Sijp et al.*, 2011], with several studies highlighting the complex nature of the long-term cooling trend during the Eocene [*Bohaty and Zachos*, 2003; *Douglas et al.*, 2014; *Scher et al.*, 2014]. Eocene reconstructions of CO_2 concentrations indicate a decline from ≥1400 ppm to ~500 ppm by the early Oligocene [*Anagnostou et al.*, 2016; *Galeotti et al.*, 2016; *Pagani et al.*, 2005, 2011]. Although deep oceans cooled during the Eocene [e.g., *Zachos et al.*, 2001], much less is known about the associated changes in circulation patterns and dominant source regions of deep water formation. Modeling and geochemical data-based studies have proposed both the Southern Ocean and the low latitudes as regions of deep water formation during the warmest periods of the Cretaceous and early Cenozoic [e.g., *Brass et al.*, 1982; *Kennett and Stott*, 1991; *Bice et al.*, 1997; *Cramer et al.*, 2009; *Hague et al.*, 2012; *Pak and Miller*, 1992; *Scher and Martin*, 2004; *Sijp and England*, 2016;

Table 1. Summary of Site and Sample Information Considered in This Study[a]

Leg	Program	Site	Hole/s	Cores	Sample Range (mbsf)	Present Location	Water Depth (m)	Paleolatitude	Paleodepth (m)
28	DSDP	264	A	3R-4R	140.30–151.35	34°58′S, 112°02′E	2873	~50°S	~2500
29	DSDP	277	-	38R-43R	389.20–435.00	52°13′S, 166°11′E	1232	~65°S	~1000
119	ODP	738	B, C	17X-24X, 6R-8R	140.95–264.70	62°42′S, 82°47′E	2253	~62°S	~1500
121	ODP	757	B	17H-21X	150.00–207.25	17°01′S, 88°10′E	1652	~40°S	~1000–1500
189	ODP	1171	D	35R-71R	565.52–912.85	48°29′S, 149°6′E	2150	~70°S	500–1000
189	ODP	1172	D	8R-14R	536.36–597.60	43°57′S, 149°55′E	2620	~65°S	500–1000
318	IODP	U1356	A	67R-106R	633.47–998.73	63°18′S, 135°59′E	4003	~65°S	500–1000

[a]See main text for references.

Thomas, 2004; *Thomas et al.*, 2014], leaving large uncertainty about the link between ocean circulation and climate during the early Cenozoic greenhouse (e.g., the early Eocene "equable climate paradox") [*Huber and Caballero*, 2011]. This is in part due to a lack of detailed records documenting Eocene climate and ocean circulation in key geographical areas.

In this study we reconstruct Southern Ocean water mass distributions during the early to middle Eocene from seven different Integrated Ocean Drilling Program (IODP), Ocean Drilling Program (ODP), and Deep Sea Drilling Project (DSDP) sites in the Tasman region, Indian Ocean, and the Southwestern Pacific Ocean using the neodymium (Nd) isotopic composition of fossil fish teeth. Neodymium is incorporated into the teeth during the fossilization process at the sediment-water interface and records the composition of bottom waters at the time of deposition [*Martin and Haley*, 2000; *Shaw and Wasserburg*, 1985]. The short residence time of Nd in seawater (~400 to 1000 years) [*Arsouze et al.*, 2009; *Tachikawa et al.*, 2003] allows the Nd isotope composition of fish teeth to be used as a tracer of prevailing water masses and ocean circulation. Our new Southern Ocean records provide insights into (i) pathways of deep and intermediate water masses during the Eocene, (ii) locations of local bottom water formation, and (iii) transient perturbations of seawater chemistry in the Southern Ocean due to changes in Antarctic climate and erosion. We suggest that the Southern Ocean acted as a major source of deep water to the surrounding ocean basins during the Eocene, highlighting the importance of this region in controlling climate even during the warmest periods of the Cenozoic.

2. Study Sites and Age Models

An overview of the study sites is presented in Table 1 and discussed in more detail below. Additional information including details of the age models used can be found in the supporting information.

2.1. Pelagic Sites

Four pelagic Southern Ocean drill sites were sampled to obtain low-resolution records of intermediate/deep water masses in the ocean basins adjacent to the Eocene Tasman Gateway region (Figure 1). Three of these sites are located in the Indian Ocean: Deep-Sea Drilling Project (DSDP) Site 264 (34°58′S, 112°02′E) [*Hayes et al.*, 1975], and Ocean Drilling Program (ODP) Sites 738 (62°42′S, 82°47′E) [*Barron et al.*, 1989] and 757 (17°01′S, 88°10′E) [*Peirce et al.*, 1989]. One additional site, DSDP Site 277 (52°13′S, 166°11′E) [*Kennett et al.*, 1975], is located in the SW Pacific. The sediments at these four pelagic sites consist predominantly of calcareous nannofossil ooze, and Eocene paleowater depths range from 1000 to 1500 m for Sites 277, 738, and 757 [*Hollis et al.*, 1997; *Roberts et al.*, 2011; *Zachos et al.*, 1992] to 2500 m for Site 264 (see supporting information). Site 738 has approximately remained at its present latitude (62°S) since the Eocene. Sites 264, 277, and 757 were located farther south than their current latitudes, at ~50°S, ~65°S, and ~40°S, respectively [*Hollis et al.*, 2015; *van Hinsbergen et al.*, 2015; *Zachos et al.*, 1992]. Age models for these sites are predominantly based on biostratigraphy with ages updated to the GTS2012 age scale [*Bohaty et al.*, 2009; *Huber and Quillévéré*, 2005; *Vandenberghe et al.*, 2012].

2.2. Shelf Sites

Three shelf sites located on both the Indian (IODP Site U1356) and Pacific (ODP Sites 1171 and 1172) sides of the Tasman Gateway (Figure 1) were included in this study. We use the age models of *Bijl et al.* [2013a] for all three of these sites, which are based on magnetostratigraphy and nannofossil and dinocyst biostratigraphy calibrated to the GTS2012 timescale.

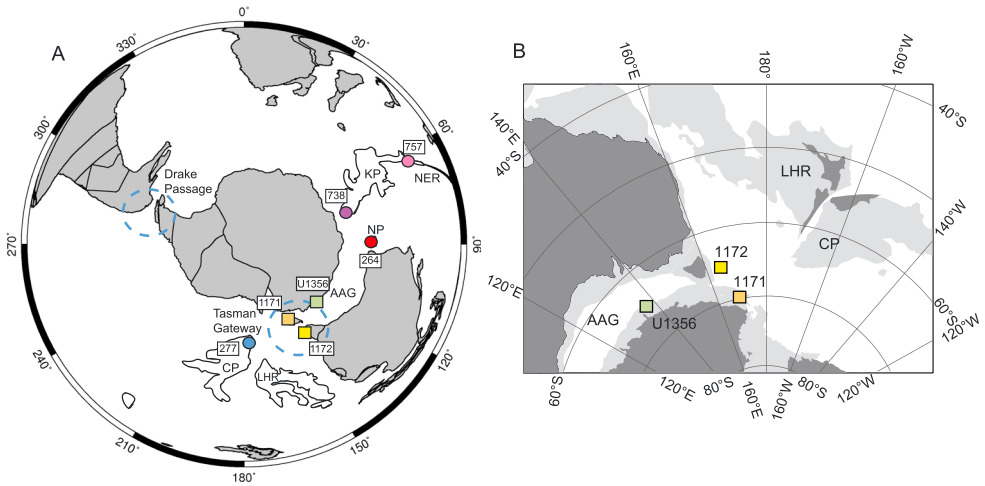

Figure 1. (a) Location of IODP/ODP/DSDP drill sites considered in this study illustrated on a 45 Ma paleogeographic reconstruction made using Ocean Drilling Stratigraphic Network online toolkit (www.odsn.de). Circles denote pelagic sites (≥1000 m), and squares denote shallow shelf sites (<500 m). Major Southern Ocean gateways are outlined with dashed lines. White outlined areas represent submerged plateaus: KP = Kerguelen Plateau, NER = Ninetyeast Ridge, NP = Naturaliste Plateau, CP = Campbell Plateau, and LHR = Lord Howe Rise. (b) Early Eocene reconstruction of shelf sites in the AAG adapted from *Bijl et al.* [2013a].

ODP Site 1171 (48°29′S, 149°6′E) on the South Tasman Rise (STR) was positioned adjacent to the Antarctic margin at ~70°S during the Eocene [*Bijl et al.*, 2013b; *Cande and Stock*, 2004]. ODP Site 1172 (43°57′S, 149°55′E) was positioned on the East Tasman Plateau (ETP) and was also located farther south at ~65°S during the Eocene [*Bijl et al.*, 2013b; *Exon et al.*, 2001]. Both sites subsided through the Eocene, with the depositional environments evolving from restricted shallow-shelf (<500 m paleodepth) to more hemipelagic (~1000 m paleodepth) conditions by the late Eocene [*Exon et al.*, 2001; *Scher et al.*, 2015].

Site U1356 (63°18′S, 135°59′E) was positioned within the enclosed Austral-Antarctic Gulf (AAG; Figure 1) during the early and middle Eocene. Progressive subsidence of the site occurred through the Eocene and Oligocene, as evidenced by lithological and dinocyst assemblage changes [*Bijl et al.*, 2013a, 2013b; *Escutia et al.*, 2011]. Existing paleodepth reconstructions suggest deepening from a shallow marine setting (~500 m paleodepth) in the early Eocene to a more hemipelagic slope setting (>1000 m) by the earliest Oligocene; however, there is a significant level of uncertainty associated with these estimates [*Escutia et al.*, 2011]. The stratigraphic sequence of Site U1356 is interrupted by two hiatuses which span from ~51 to 49 Ma and from ~46 to 33.6 Ma [see *Bijl et al.*, 2013b; *Houben et al.*, 2013; *Tauxe et al.*, 2012]. For the purposes of our study, the three hiatus-bound sedimentary packages recovered at Site U1356 will be designated according to age and referenced to as follows: the early Eocene (1006.4 to 948.8 meters below seafloor (mbsf); ~54 to 51.5 Ma), "mid"-Eocene (948.8 to 894.68 mbsf; ~49 to 46 Ma), and Oligocene (894.68 to 633.47 mbsf; ~33.5 to 25 Ma).

3. Methods

3.1. Neodymium Isotopes

3.1.1. Fossil Fish Tooth Sample Preparation

A total of 41 samples across all study sites were prepared for fish tooth Nd isotope analyses for this study. We also include data from an additional 25 fish tooth samples analyzed from mid-Eocene Core U1356A-98R [*Huck et al.*, 2016]. Fossil fish teeth were picked from the >63 μm sediment fractions that were prepared by wet sieving. To test whether a full oxidative-reductive cleaning protocol was necessary for fish tooth analysis, two samples each from Site U1356, Site 1171, and Site 1172, reflecting a range of ages, different sediment compositions, and paleowater depths, were split into two aliquots. One sample split (referred to as "cleaned") was subjected to a full oxidative-reductive cleaning protocol to remove Fe-Mn oxyhydroxide coatings using the method adapted from *Boyle and Keigwin* [1985]. The other split ("uncleaned") was treated with the simplified MQ-water and methanol-only cleaning method of *Martin and Haley* [2000] (supporting information Table S1). Cleaned fish tooth samples were subsequently dissolved overnight in 2 *M* HCl. A fossil bone

composite standard was used for quality control and was digested following the method described in *Chavagnac et al.* [2007]. In short, the fish tooth and bone standard was digested by dissolving 50 mg of material in 3 *M* HNO_3 in a sealed Teflon beaker on a hotplate at 130°C. Any residue remaining after this step was subjected to a further 48 h digestion in a 3:1 mixture of 15 *M* HNO_3 and 27 *M* HF. Neodymium from all samples was then collected using a standard two-stage ion exchange chromatography to first separate the rare earth elements (REEs) from the sample matrix using TRU-Spec resin (100–120 μm bead size) and to then isolate Nd from the other REEs using Ln-Spec resin (50–100 μm bead size) (modified after *Pin and Zalduegui* [1997]).

3.1.2. Bulk Sediment Sample Preparation

Bulk sediment Nd isotopic composition was determined for 12 samples from Site U1356 and four samples from Site 1171. A further six bulk sediment samples from mid-Eocene core U1356A-98R from *Huck et al.* [2016] are also included in the sample set. For these analyses, 0.5–1.0 g of sediment was oven dried, completely homogenized using a mortar and pestle, and ~100 mg of the powdered sample was weighed and digested using a mixture of 0.5 mL 20 *M* $HClO_4$, 1 mL 15 *M* HNO_3, and 3 mL 27 *M* HF. Fe-Mn coatings were not removed from the sediment samples in our study, as previous work on Eocene-aged samples at Site U1356 has shown the contributions from authigenic phases to the final Nd isotopic composition to be negligible (i.e., <1% total signal) [*Huck et al.*, 2016]. The bulk samples were processed using the same column chemistry used for the fish teeth.

3.1.3. Neodymium Isotope Measurements

Neodymium isotope ratios for fish tooth and sediment samples were determined at Imperial College London on a Nu Plasma multi-collector inductively coupled plasma mass spectrometer operated in static mode (supporting information Table S1). We used a $^{146}Nd/^{144}Nd$ ratio of 0.7219 to correct for instrumental mass bias. Samarium (Sm) interference can be adequately corrected if the ^{144}Sm signal contributes less than 0.1% of the ^{144}Nd signal. The Sm contribution in all our samples was well below this level. Replicate analyses of the Nd standard JNdi [*Tanaka et al.*, 2000] yielded $^{143}Nd/^{144}Nd$ ratios from 0.511937 ± 0.000015 to 0.512251 ± 0.000015 (2σ, $n = 316$) depending on daily running conditions over 29 months. External reproducibility of sediment samples was monitored using USGS rock standards BCR-1 and BCR-2, which yielded ratios from 0.512651 ± 0.000014 to 0.512655 ± 0.000022 and from 0.512632 ± 0.000016 to 0.512649 ± 0.000016, respectively. These values are indistinguishable from the ratios published by *Weis et al.* [2006] (BCR-1: 0.512646 ± 0.000016; BCR-2: 0.512638 ± 0.000015). The fossil bone composite standard yielded a $^{143}Nd/^{144}Nd$ ratio of 0.512377 ± 0.000014 (2σ, $n = 8$), which agrees within error with ratios published by *Chavagnac et al.* [2007] and *Scher and Delaney* [2010]. Procedural blanks were consistently below 10 pg.

To correct for the decay of ^{147}Sm to ^{144}Nd within the fish teeth over time we used Sm and Nd concentrations obtained from one or more samples at every site (supporting information Table S2). $^{147}Sm/^{144}Nd$ ratios for all samples are between 0.124 and 0.174 and are consistent with values for Cretaceous to Miocene fossil fish tooth material [*Martin and Scher*, 2006; *Moiroud et al.*, 2013; *Thomas et al.*, 2003]. These maximum and minimum $^{147}Sm/^{144}Nd$ ratios would yield a difference of between 10 and 30 ppm if applied to $\varepsilon_{Nd(t)}$ calculations for the same samples, which is within the external reproducibility reported. We therefore applied a site-specific average value ($^{147}Sm/^{144}Nd = 0.128$ to 0.153) to all samples and denote all ^{147}Sm decay-corrected Nd isotope data as $\varepsilon_{Nd(t)}$ (where ε_{Nd} is the deviation of the $^{143}Nd/^{144}Nd$ ratio measured in a sample from that of the chondritic uniform reservoir in parts per 10,000 [*Jacobsen and Wasserburg*, 1980] and $_{(t)}$ denotes the sample correction for radiogenic ingrowth over time).

3.2. Rare Earth Elements

The full suite of REE concentrations were determined for 10 fossil fish tooth samples from the early Eocene and Oligocene sections from Site U1356 and are compiled with a further 16 mid-Eocene samples from *Huck et al.* [2016]. Two samples each from Sites 1171 and 1172 and one sample each from Sites 757, 738, 264, and 277 were also analyzed. Major and trace element analysis was performed at the Open University using an Agilent 7500s ICP-MS (supporting information Table S2). Oxide interferences were kept below 0.3% for CeO^+/Ce^+ and 0.8% for (Ce^{++}/Ce^+). Analyses were standardized against seven synthetic reference materials selected for their similarity to the samples that were measured at the beginning and end of each analytical run. Detection limits for elements with atomic masses greater than 85 were typically <10 ppt in solution but were somewhat higher for lighter elements (10–100 ppt in solution). Precision was routinely better than ±2% for elements heavier than rubidium (Rb) (where concentrations exceed 0.5 ppm) and 2–4% for

lighter elements. All sample REE data were normalized to Post Archean Shale (PAAS) concentrations [*Taylor and McLennan*, 1985]. The Ce anomaly for fish tooth samples (Ce/Ce*) was calculated following *De Baar et al.* [1985], where $Ce/Ce^* = 2Ce_n/(La_n + Pr_n)$.

4. Results

4.1. Fossil Fish Tooth Nd Isotopic Compositions

$\varepsilon_{Nd(t)}$ values of fish tooth samples from all pelagic sites in this study yield an average value of −9.1 ± 1.6 (2sd, n = 19). Indian Ocean Sites 264, 738, and 757 range from −10.7 to −7.8 within the time interval between ~52 and 44 Ma (average $\varepsilon_{Nd(t)}$ = 9.3 ± 1.5, 2sd, n = 13; supporting information Table S1 and Figure 2). The most unradiogenic values at Sites 738 and 757 ($\varepsilon_{Nd(t)}$ = −10.7 and −9.8, respectively) occur between ~50 and 48.5 Ma, with increasingly radiogenic compositions recorded at these sites between ~48 and 44 Ma. The three fish tooth samples from Site 264 have a similar isotopic composition ($\varepsilon_{Nd(t)}$ = −9.6 to −9.1). $\varepsilon_{Nd(t)}$ values of fish tooth samples from the pelagic SW Pacific Site 277 range from −9.7 to −7.3 between ~53 and ~47 Ma (average $\varepsilon_{Nd(t)}$ = −8.7 ± 1.7, 2sd, n = 6). The most negative $\varepsilon_{Nd(t)}$ value of −9.7 recorded at Site 277 occurs at ~49 Ma (Figure 2).

$\varepsilon_{Nd(t)}$ values of early to middle Eocene-aged fish tooth samples at shelf Sites 1171 and 1172 span a range of −8.9 to −5.3. The most negative Nd isotopic composition recorded at Site 1172 occurs at ~50 Ma ($\varepsilon_{Nd(t)}$ = −7.9), whereas the fish tooth $\varepsilon_{Nd(t)}$ record at Site 1171 contains two negative excursions to minimum values of −8.9 at ~48.7 Ma and −8.2 at ~47.8 Ma (Figure 2). Including previously published data from *Huck et al.* [2016], compiled fish tooth $\varepsilon_{Nd(t)}$ values spanning the early Eocene to Oligocene (~54 to ~25 Ma) at IODP Site U1356 span a range of ~3 epsilon units ($\varepsilon_{Nd(t)}$ = −9.6 to −12.4) (Figure 2 and supporting information Table S1). Early Eocene fish teeth at Site U1356 have an average Nd isotope $\varepsilon_{Nd(t)}$ value of −10.7 ± 1.0 (2sd, n = 11). During the mid-Eocene interval, a negative excursion to a minimum value of −12.4 is observed at 48.2 Ma. Within the Oligocene section of Site U1356, $\varepsilon_{Nd(t)}$ values vary by 1 epsilon unit between −10.2 and −11.2 with an average value of −10.7 ± 0.8 (2sd, n = 8), similar to the average early Eocene value.

4.2. Site U1356 and Site 1171 Bulk Sediment Nd Isotopic Compositions

At Site U1356, the Nd isotopic composition of bulk sediment samples from the early to mid-Eocene interval (~47 to 53 Ma) of this study and *Huck et al.* [2016] span a narrow range of ~1.7 epsilon units (−13.1 to −14.8) (Figure 3 and supporting information Table S1). These bulk sediment values are more negative than fish tooth $\varepsilon_{Nd(t)}$ values by at least 2 epsilon units throughout the study section (Figure 3 and supporting information Table S1) [*Huck et al.*, 2016]. Across the early to middle Eocene (~49 and 47.5 Ma) interval of Site 1171, the Nd isotopic composition of bulk sediment shows limited variability ($\varepsilon_{Nd(t)}$ = −9.3 to −9.8) in contrast to the large amplitude variations observed in fish tooth samples. Similar to the results obtained from Site U1356, the bulk sediment $\varepsilon_{Nd(t)}$ values at Site 1171 are lower than the value obtained from fish teeth from the same interval (Figure 3) by ~2 epsilon units.

4.3. Fossil Fish Tooth REE Patterns

The REE patterns of fossil fish tooth samples were primarily generated to confirm a seawater-derived signal for Nd in all of our samples. Fish tooth samples from pelagic Sites 738, 757, 277, and 264 yielded middle-REE enriched patterns with a pronounced negative Ce anomaly (Ce/Ce* = 0.3 to 0.6) and a positive yttrium (Y) anomaly (Figure 4). Such patterns, as well as low overall REE concentrations, are diagnostic of a seawater origin [e.g., *German and Elderfield*, 1990; *Scher et al.*, 2011]. The fish tooth REE patterns from shelf Sites 1171, 1172, and U1356 show a similar enrichment in mid-REEs but a positive Ce anomaly (Ce/Ce* = 1.0 to 1.9) (Figure 4). The positive Ce anomalies may arise from increased weathering of proximal continental regions and/or remobilized REEs from authigenic or organic coatings [e.g., *Elderfield and Pagett*, 1986; *Freslon et al.*, 2014; *Huck et al.*, 2016; *Wright et al.*, 1987]. Oligocene fish tooth REE concentrations at Site U1356 (gray color in Figure 4 and supporting information Table S2) are generally more enriched than those of the Eocene samples (dark and light green color in Figure 4 and supporting information Table S2). All cleaned and uncleaned fish tooth samples from pelagic and shelf sites show similar REE patterns, with cleaned samples having consistently lower REE concentrations (supporting information Table S2).

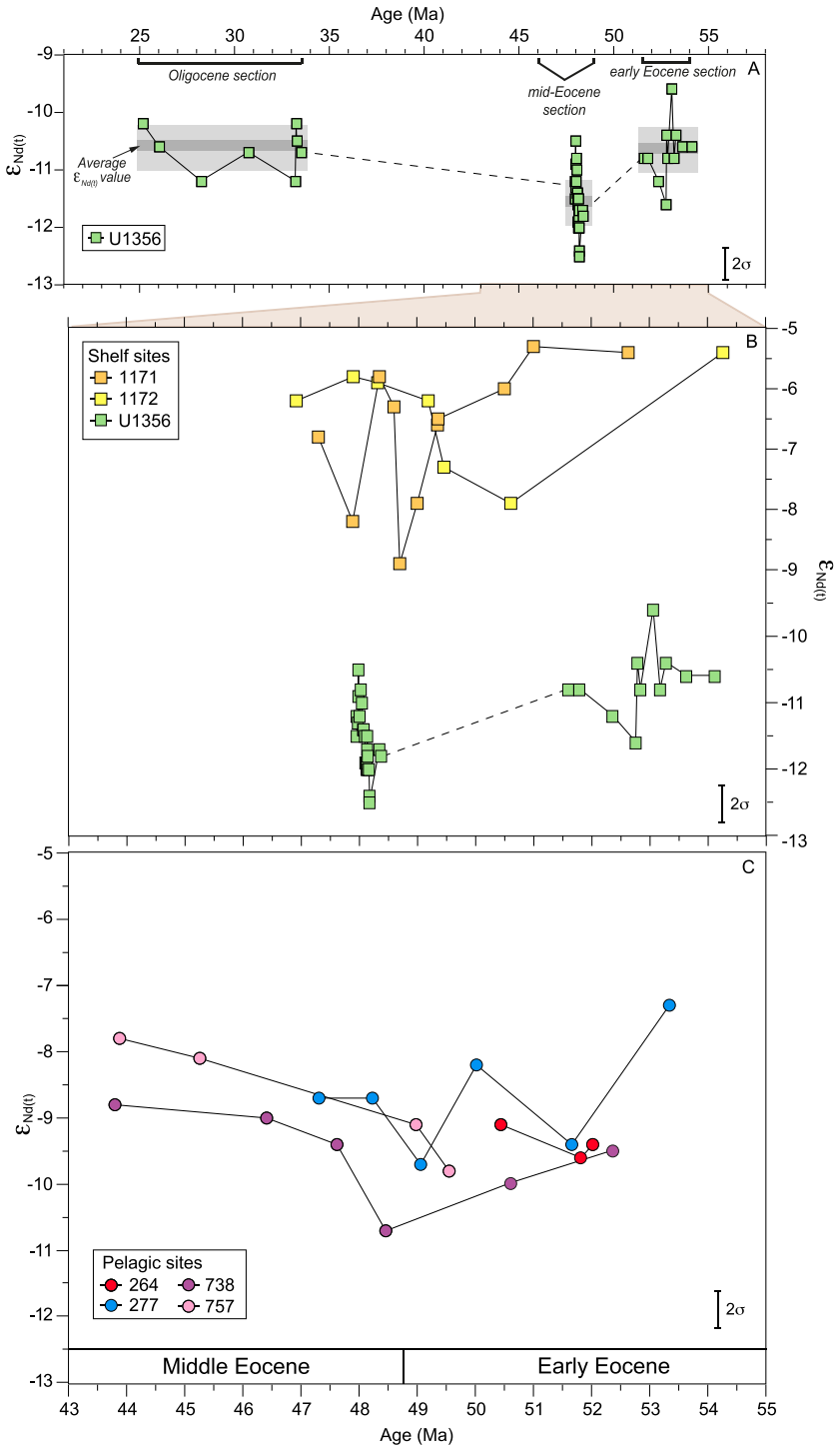

Figure 2. (a) Eocene-Oligocene Nd isotopic composition of fossil fish teeth and debris at Site U1356 from this study and *Huck et al.* [2016]. (b) Early to middle Eocene Nd isotope data for fossil fish tooth samples from shallow Sites 1171 (orange squares) and 1172 (yellow squares) and U1356 (light green squares). (c) Pelagic Sites 757 (pink circles), 738 (purple circles), 264 (red circles), and 277 (blue circles).

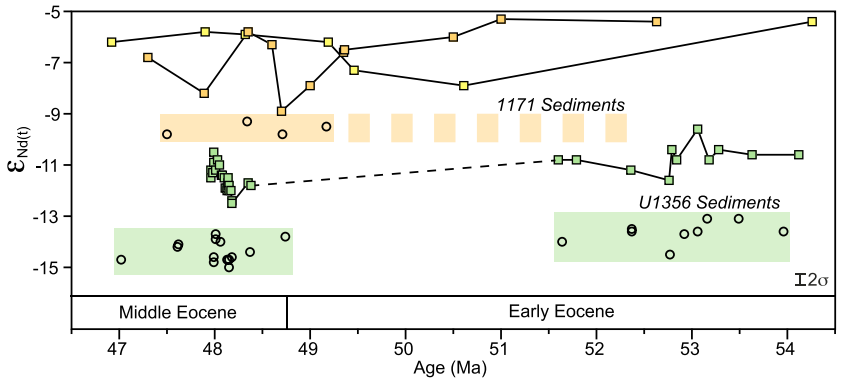

Figure 3. Neodymium isotopic composition of fossil fish teeth and debris at shelf Sites U1356 (green squares), 1171 (orange squares), and 1172 (yellow squares). Bulk sediment $\varepsilon_{Nd(t)}$ values (open circles) are indicated by the corresponding orange (Site 1171) and green (Site U1356) bars. Sediment data for Site U1356 are from this study and *Huck et al.* [2016].

5. Discussion

To evaluate ocean circulation in the Southern Ocean during the Eocene, we separate our study sites into two geographical provinces: (i) those located in the Indian Ocean sector of the Southern Ocean situated to the west of the Tasman Gateway and (ii) sites from the Pacific sector of the Southern Ocean to the east of the Tasman Gateway. Interpreted circulation patterns and history derived from these records are then synthesized and discussed in the context of the cooling trend that followed the maximum warmth of the EECO.

5.1. Eocene Circulation and Origin of Deep Water Masses in the Indian Ocean Sector of the Southern Ocean

Fish tooth Nd isotope records have previously been reported for Indian Ocean Site 757 ($\varepsilon_{Nd(t)} = -6.0$ to -7.5; 34–40 Ma) [*Martin and Scher*, 2006] (Figure 5) and Sites 689 and 1090 in the Atlantic sector of the Southern Ocean ($\varepsilon_{Nd(t)} = -5.2$ to -9.5; 34–46 Ma) [*Scher and Martin*, 2004, 2006] (Figure 5). Our new fish tooth Nd isotope records extend these records from 43.8 Ma to 52 Ma and overlap with previously published $\varepsilon_{Nd(t)}$ values between 43.8 and 46 Ma ($\varepsilon_{Nd(t)} = -8.8$ to -9.0 and -7.8 to -8.1 for sites 738 and 757 respectively; supporting information Table S1 and Figure 5). However, more unradiogenic compositions (i.e., lower $\varepsilon_{Nd(t)}$ values) are observed throughout the early to middle Eocene than previously recorded in the Indian Ocean during the Eocene, with minimum $\varepsilon_{Nd(t)}$ values of -9.6 to -10.7 across all sites (Figure 2).

Eocene seawater $\varepsilon_{Nd(t)}$ values below -9.5 have previously been documented only in fish debris and ferromanganese crust records from the North Atlantic ($\varepsilon_{Nd(t)}$ -7.1 to -10.5) [*Burton et al.*, 1997; *Thomas et al.*, 2003] (Figure 6). *Hohbein et al.* [2012] proposed formation of deep water in the North Atlantic Basin from the early to middle Eocene transition, but significant southward export of these waters to equatorial Atlantic areas has only been detected from the late Eocene [*Borrelli et al.*, 2014]. Therefore, it seems unlikely that a significant contribution of unradiogenic Nd was transported to our Indian Ocean study sites from the North Atlantic during the early and middle Eocene. This argument is further supported by the subsidence history of Ninety East Ridge and the Kerguelen Plateau which allowed the exchange of intermediate waters between the east and west Indian Ocean basins by the Eocene [e.g., *Zachos et al.*, 1992] but may have restricted the flow of deeper waters from entering the east Indian Ocean.

Another possible source of deep water to the Indian and Southern Oceans during the Eocene may have been the Tethys Ocean [e.g., *Kennett and Stott*, 1991; *Scher and Martin*, 2004]. Limited Nd isotope data for seawater in the Tethys during the Eocene are derived from glauconitic deposits in Northern Europe ($\varepsilon_{Nd(t)} = -9.3$ to -9.8) [*Stille and Fischer*, 1990] and phosphate-bearing carbonates in southern Israel ($\varepsilon_{Nd(t)} = -7.5$) [*Soudry et al.*, 2006]. Export of waters with this range of $\varepsilon_{Nd(t)}$ values from the Tethys may explain our fish tooth record at Site 757, but not at Site 738, which reaches $\varepsilon_{Nd(t)}$ values as low as -10.7 (Figure 5). Furthermore, early Eocene benthic foraminifer $\delta^{18}O$ reconstructions from Sites 757 and 738 are consistent with a southern sourced, cooler water mass [*Zachos et al.*, 1992] rather than a warmer water mass originating at low latitudes.

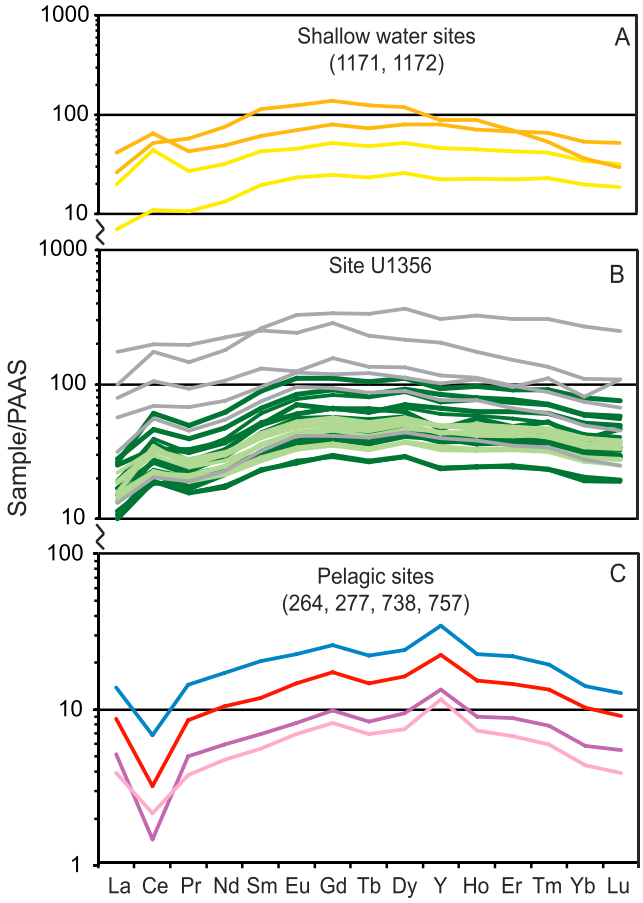

Figure 4. Rare earth element (REE) patterns normalized to PAAS [*Taylor and McLennan*, 1985] for (a) shallow water Sites 1171 (orange) and 1172 (yellow), (b) Wilkes Land Site U1356 Early Eocene (green; this study, <500 m water depth) to mid-Eocene (dark green; this study and *Huck et al.* [2016]) and Oligocene intervals (gray, ~1000 m water depth), and (c) pelagic sites 757 (pink), 738 (purple), 264 (red), and 277 (blue).

The early to middle Eocene $\varepsilon_{Nd(t)}$ values recorded by fossil fish teeth at Indian Ocean Sites 264, 738, and 757 are similar to modern-day bottom waters forming along the Antarctic margin in regions such as the Wilkes Land-Adélie Coast ($\varepsilon_{Nd} = -9.3$ to -10.5) [*van de Flierdt et al.*, 2006; *Lambelet et al.*, 2014]. This unradiogenic composition reflects the influence of Archean and Proterozoic bedrock outcropping along the Wilkes Land and Adélie Coast margin [e.g., *Pierce et al.*, 2011, 2014]. Average fish tooth $\varepsilon_{Nd(t)}$ values of the Wilkes Land/Adélie Coast Site U1356 during the early Eocene and Oligocene are -10.7 ± 1.0 (2sd, $n = 11$) and -10.6 ± 0.8 (2sd, $n = 8$), respectively (supporting information Table S1 and Figure 2), and are relatively invariant through time despite progressive deepening of the site from a shallow marine to hemipelagic slope environment (>1000 m) during the Eocene [e.g., *Escutia et al.*, 2011; *Lawver and Gahagan*, 2003]. A stable Nd isotopic composition over a range of depths at Site U1356 is consistent with modern day observations of the formation of bottom water off the Adélie Coast. A source of locally forming waters on the Wilkes Land-Adélie Coast margin during the Eocene provides a suitable Nd end-member for the unradiogenic Nd compositions reconstructed at the Indian Ocean pelagic sites in this study.

The modern process of AABW production from modified Antarctic Surface Water (AASW) and Circumpolar Deep Water (CDW) via sea ice formation and winter cooling [e.g., *Orsi and Wiederwohl*, 2009] would not have been possible during the persistant Antarctic warmth of the early Eocene [e.g., *Pross et al.*, 2012]. However, modeling studies suggest that Cretaceous to Eocene deep water formation and downwelling may have occurred due to density contrasts created by seasonal changes in surface water temperatures and salinity (with or without the presence of sea ice) [e.g., *Lunt et al.*, 2010; *Huber and Sloan*, 2001; *Otto-Bliesner et al.*,

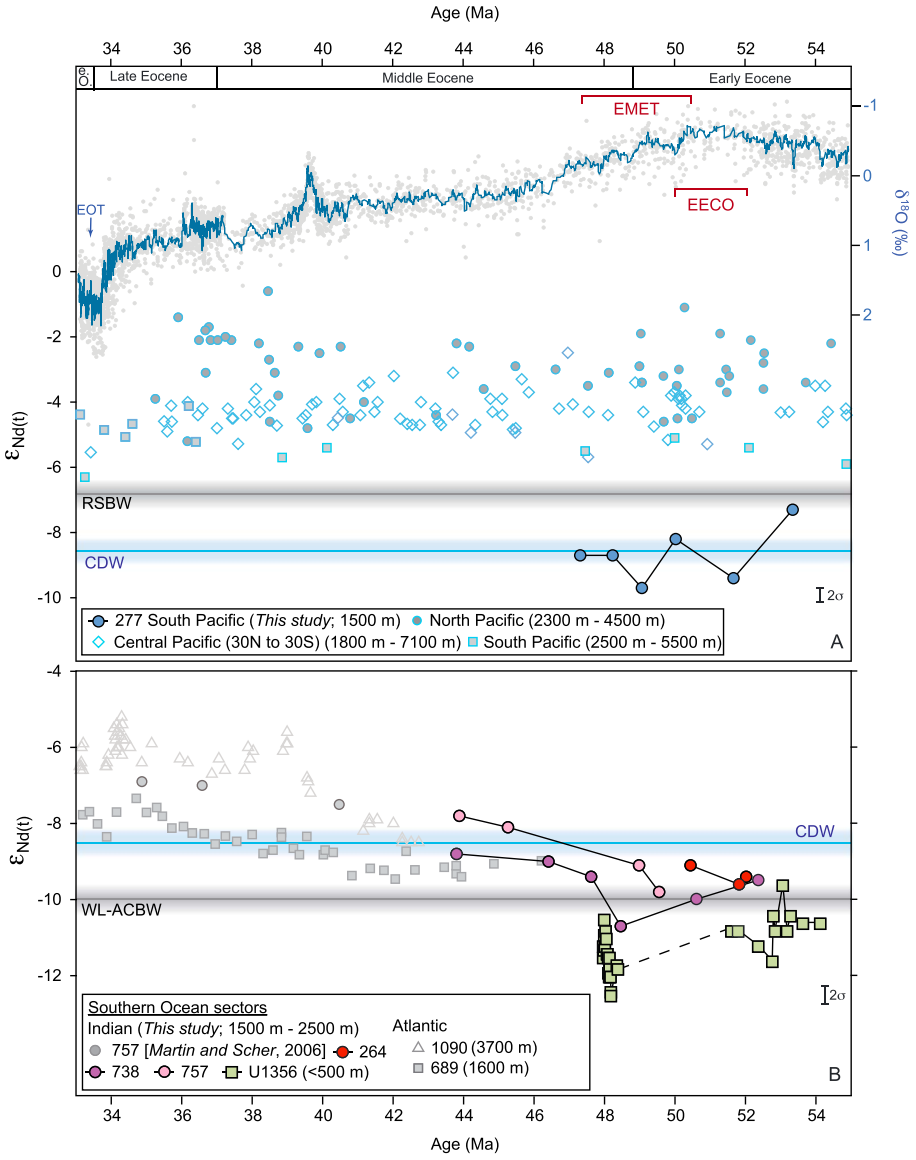

Figure 5. Compilation of (i) published Eocene authigenic Nd isotope data for the (top) Pacific (gray data points) and (bottom) Atlantic/Indian sectors of the Southern Ocean (gray data points) and (ii) new data generated for this study (pelagic sites only; colored data points). Global benthic foraminifer $\delta^{18}O$ stack from *Cramer et al.* [2009] (Figure 5, top). North Pacific data: *Hague et al.* [2012] and *Thomas* [2004]. Equatorial Pacific data: *Thomas et al.* [2008, 2014], *van de Flierdt et al.* [2004], *Ling et al.* [1997, 2005], and *Le Houedec et al.* [2016]. South Pacific data: *Thomas et al.* [2014], *Scher et al.* [2015], and this study. Atlantic/Indian Ocean data: *Martin and Scher* [2006], *Scher and Martin* [2004, 2006], *Thomas et al.* [2003], and this study. Modern day Ross Sea Bottom Water (RSBW, gray shading) and Circumpolar Deep Water (CDW, blue shading) ε_{Nd} values taken from *Rickli et al.* [2014] and *Stichel et al.* [2012]. Modern Wilkes Land/Adélie Coast Bottom Water (WL-ACBW, gray shaded bar) ε_{Nd} values from *Lambelet et al.* [2014].

2002]. More recently, *Sijp and England* [2016] demonstrated that reduced pole-to-equator sea surface temperature gradients, such as those reconstructed from the Tasman Gateway region during the early Eocene [e.g., *Bijl et al.*, 2009], had little effect on modeled ocean circulation patterns or deep water formation in the southern high latitudes.

Two final observations from our fish tooth Nd data support the persistent export of deep waters from the Antarctic shelves during the early to middle Eocene: (1) the Nd isotope records from high-latitude Site 738 and more northerly Site 757 (Figure 1) follow the same trend towards more radiogenic $\varepsilon_{Nd(t)}$ values during the early to middle Eocene and (2) a consistent Nd isotope gradient of ~1 ε_{Nd} unit exists between these

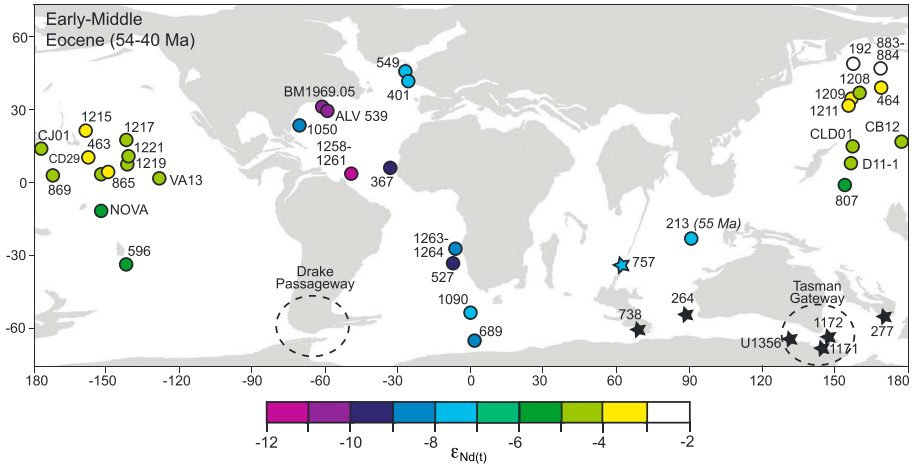

Figure 6. Global sites from the Atlantic, Indian, Pacific, and Southern Ocean basins, where seawater Nd isotope data have been generated for the early to middle Eocene time interval (~54–40 Ma). Data from literature denoted using circles color coded by Nd isotopic composition. New data generated in this study denoted by stars. The published ≤40 Ma record for Site 757 [*Martin and Scher*, 2006] has been extended in this study back to the early Eocene. Atlantic Ocean data: *Scher and Martin* [2006], *Scher and Martin* [2004], *Via and Thomas* [2006], *Thomas et al.* [2003], *MacLeod et al.* [2011], *Martin et al.* [2012], *Burton et al.* [1997], and *O'Nions et al.* [1998]. Indian Ocean data: *Martin and Scher* [2006] and *Thomas et al.* [2003]. Pacific Ocean data: *Ling et al.* [1997, 2005], *Hague et al.* [2012], *Thomas* [2004], and *Thomas et al.* [2008, 2014]. Tectonic reconstruction made using Ocean Drilling Stratigraphic Network online toolkit (www.odsn.de).

two sites across a south-to-north transect, with lower values at southern Site 738 (Figure 5), suggesting a source to the south. We speculate that entrainment and export of Antarctic shelf-sourced waters to the Indian Ocean study sites likely occurred in geostrophically driven deep western boundary currents [e.g., *Scher et al.*, 2014] (Figure 7) and is consistent with several proxy-based [e.g., *Corfield and Norris*, 1996; *Cramer et al.*, 2009; *Katz et al.*, 2011; *Pak and Miller*, 1992; *Sexton et al.*, 2006; *Zachos et al.*, 1992, 1994] and model-based studies [e.g., *Bice et al.*, 1997; *Douglas et al.*, 2014; *Uenzelmann-Neben et al.*, 2016].

5.2. Eocene Circulation and Origin of Deep Water Masses in the Southwest Pacific

Fish tooth $\varepsilon_{Nd(t)}$ values from Site 277 in the SW Pacific sector of the Southern Ocean range from −7.3 to −9.7 and are similar to those recorded at Indian Ocean sites but are ~2 epsilon units lower on average than Eocene $\varepsilon_{Nd(t)}$ values from other Pacific Ocean sites ($\varepsilon_{Nd(t)}$ = −1.8 to −6.3 between 34 and 55 Ma) [*Le Houedec et al.*, 2016; *Ling et al.*, 1997, 2005; *Hague et al.*, 2012; *Thomas*, 2004; *Thomas et al.*, 2008, 2014; *Scher et al.*, 2015; *van de Flierdt et al.*, 2004] (Figures 5 and 6). This observation is noteworthy, as the Tasman Gateway was fully closed or only open to very shallow circulation during the early and middle Eocene [*Bijl et al.*, 2013b]. Changes in dinoflagellate assemblages at Site U1356 between 48 and 49 Ma [*Bijl et al.*, 2013b] have been interpreted as a shallow opening of the Tasman Gateway, with waters flowing from the SW Pacific into the AAG under the influence of prevailing winds from the east [e.g., *Huber et al.*, 2004]. Furthermore, younger fish tooth Nd isotope records from the region indicate an intermediate to deep (~500 to 2500 m) water flow from the Pacific to the Indian Ocean through the gateway in the late Eocene. Consistent with these observations, we note that the negative $\varepsilon_{Nd(t)}$ values recorded at Site 277 during the early to middle Eocene predate even the earliest opening event in the region. We conclude that it is unlikely that the unradiogenic intermediate/deep waters at Site 277 were the result of eastward transport from the Indian Ocean sector through the Tasman Gateway to the Ross Sea region during the early to middle Eocene.

Instead, we propose two alternative options for the unradiogenic character of waters at Site 277: (1) an influx of intermediate/deep waters from the Indian Ocean via the Indonesian seaway or (2) local formation of intermediate/deep waters in the Ross Sea region. Through the Cretaceous to Eocene, the low-latitude seaways were characterized by a strong, westward flowing surface current. These waters flowed from the Pacific Ocean through the Indonesian seaway and across continental seaways in the Tethys to the Atlantic basin [e.g., *Jovane et al.*, 2009; *Pucéat et al.*, 2005; *Poulsen et al.*, 1999; *Soudry et al.*, 2006]. Radiogenic

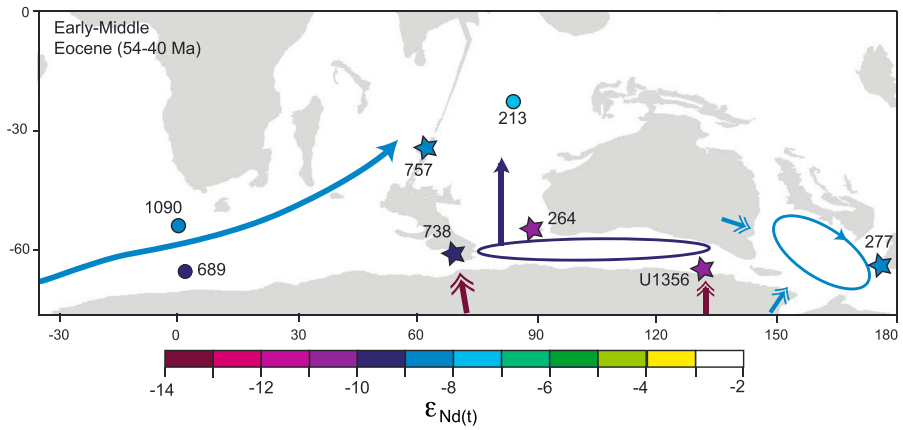

Figure 7. Simplified intermediate/deep water mass circulation in the Southern Ocean during the early to middle Eocene as interpreted from this study. Study sites (stars) and water masses (arrows) are color coded to average $\varepsilon_{Nd(t)}$ values from this study for the 54–40 Ma interval, with the exception of Sites 689 and 1090 (~40–43 Ma) [*Scher and Martin*, 2004, 2006, 2008] and Site 213 [*Thomas et al.*, 2003]. Double-headed arrows represent $\varepsilon_{Nd(t)}$ values of Eocene sediment from Antarctic and Australian hinterland [*Cook et al.*, 2013; *Gingele and De Deckker*, 2005; this study]. Tectonic reconstruction made using Ocean Drilling Stratigraphic Network online toolkit (www.odsn.de).

seawater Nd isotope compositions are reconstructed at depth from the Pacific side of the Indonesian Gateway throughout the Eocene ($\varepsilon_{Nd(t)}$ = −5.9 to −4.6) [*Le Houedec et al.*, 2016], in contrast to more unradiogenic values reconstructed at Site 213 in the Indian Ocean [*Thomas et al.*, 2003] (Figure 6). A consistent radiogenic-unradiogenic trend from the Pacific to the Indian Ocean basins suggests a westward flow of intermediate/deep waters also characterized the region during the Eocene. We therefore consider Indian Ocean waters flowing through the Indonesian seaway an unlikely explanation for the unradiogenic Nd values recorded at SW Pacific Site 277.

The dominantly radiogenic Nd isotopic composition of Pacific deep waters during the Eocene (Figure 5) have persisted since at least ~110 Ma [e.g., *Robinson et al.*, 2010] and reflect the influx of Nd from young volcanic rocks around the Pacific rim [e.g., *Goldstein and Jacobsen*, 1988; *Jeandel et al.*, 2007]. In contrast, outcropping bedrock around the pre-Eocene continental margins of the SW Pacific contains a significant amount of older terranes (i.e., Proterozoic basement and Paleozoic granitoids and metasediments of the Australian and Antarctic margins) [*Cook et al.*, 2013; *Pankhurst et al.*, 1998; *Roberts et al.*, 2013] as well as younger Mesozoic volcanics, providing a range in ε_{Nd} values that extends to quite unradiogenic Nd isotopic compositions ($\varepsilon_{Nd(t)}$ ~ −4 to −20) [*Cook et al.*, 2013; *Gingele and De Deckker*, 2005]. This range of bedrock Nd compositions provides a suitable source region for the seawater Nd isotopic compositions recorded at Site 277 (Figure 5).

Based on the distribution of geological source regions surrounding the Pacific Ocean basin, the unradiogenic character of fish tooth Nd isotope values from Site 277 suggests formation of intermediate/deep waters in the SW Pacific region during the early and middle Eocene, most likely the Ross Sea region, in agreement with existing modeling and proxy-based studies [e.g., *Hollis et al.*, 2012; *Huber et al.*, 2004; *Thomas et al.*, 2014]. We also note that fish tooth ε_{Nd} records from the Central Pacific suggest a significant contribution of unradiogenic deep waters (paleodepths of 2300 to 2900 m) originating from the Ross Sea (South Pacific Deep Water, SPDW) during the early Eocene [e.g., *Thomas et al.*, 2003, 2014].

However, Site 277 $\varepsilon_{Nd(t)}$ values (−7.3 to −9.7) are lower than both Eocene seawater Nd isotope distributions modeled by *Thomas et al.* [2014] for the SW Pacific ($\varepsilon_{Nd(t)}$ = ~ − 6.5 to −6.0) and modern day values of Ross Sea bottom water (ε_{Nd} = −7.4 to −6.5) [*Rickli et al.*, 2014]. One possible explanation is that the Nd isotopic composition of RSBW has changed through time. This is feasible due to the Oligocene, and younger, emplacement ages of the late Cenozoic McMurdo Volcanic Group in broad areas around the Ross Sea [e.g., *McIntosh*, 2000]. Clear evidence for a major change in the composition of erosional inputs to the Ross Sea, containing material from this young, volcanic source, is provided in the Cape Roberts cores [*Roberts et al.*, 2013] and could have readily affected local seawater, driving it toward more radiogenic

Nd isotopic compositions since the Oligocene/Miocene. Unfortunately, there are currently no Eocene-aged deep/bottom water Nd data (>1500 m paleodepth) from the SW Pacific region, and, as such, we are unable to conclude whether the intermediate/deep waters at Site 277 were ultimately exported from the region as deeper flowing SPDW or whether a more stratified water column prevailed with unradiogenic waters reconstructed from Site 277 overlying a more radiogenic proto-RSBW [e.g., *Thomas et al.*, 2014].

5.3. The Role of Ocean Circulation in the Termination of the EECO

A notable feature of our new early and middle Eocene fish tooth Nd records is the occurrence of a pronounced excursion in $\varepsilon_{Nd(t)}$ values between 50 and 48 Ma at multiple sites located in the southern Indian Ocean, Australo-Antarctic Gulf, and SW Pacific Ocean. The most unradiogenic Nd isotopic compositions are observed at Sites 738, 757, 1171, and U1356 and coincide with the end of extreme global warmth during the EECO, falling within the early/middle Eocene Transition (EMET; ~51–47 Ma; Figure 5). The EMET is characterized by global cooling of deep ocean temperatures, sea level lowstands, and widespread deep marine sediment hiatuses [e.g., *Browning et al.*, 1996; *Hohbein et al.*, 2012; *Kominz et al.*, 2008; *Miller et al.*, 1987; *Pekar et al.*, 2005; *Zachos et al.*, 2008]. A drop in atmospheric pCO_2 concentrations, potentially driven by increased silicate weathering, may explain global cooling [e.g., *Anagnostou et al.*, 2016; *Kent and Muttoni*, 2008, 2013], while tectonic reorganization such as the shallow opening of the Tasman Gateway at ~48 Ma may have also caused regional cooling [*Bijl et al.*, 2013b]. Below we further explore the origin of the fish tooth Nd excursions from sites in the Tasman Gateway region and the potential relationship between these excursions and the cooling climate trend following the EECO.

5.3.1. Shallow Opening of the Tasman Gateway

Based on early to middle Eocene marine microfossil and organic geochemical records from Site U1356, *Bijl et al.* [2013b] interpreted a shallow opening of the Tasman Gateway during the EMET. The associated influx of Pacific-sourced surface waters to the Australo-Antarctic Gulf is proposed to have resulted in regional cooling along the East Antarctic margin. There was likely long-term deepening of Site U1356 from ~500 m to ~1000 m during the early to middle Eocene [*Bijl et al.*, 2013b; *Escutia et al.*, 2011], but precise paleodepth estimates for the site are uncertain. Given the uncertainty of the paleodepth of Site U1356 at the EMET, it is possible that a shallow influx of Pacific waters through the Tasman Gateway may not have been detected in our fish tooth Nd isotope record. If the arrival of Pacific-sourced waters was captured by fish tooth samples at Site U1356, we would expect a step change in Nd isotopes toward more radiogenic compositions, similar to $\varepsilon_{Nd(t)}$ values observed at Sites 1171 and 1172 (which have average Eocene $\varepsilon_{Nd(t)}$ values of -6.6 ± 2.2 (2sd, $n = 23$)). We do not observe such as shift during the mid-Eocene interval at Site U1536, but instead a transient excursion to unradiogenic compositions in fish tooth Nd isotopes away from, and subsequently returning to, the average Nd isotopic composition defined by the early Eocene and Oligocene sections of the record (Figure 2). This suggests that a different mechanism than the shallow opening of the Tasman Gateway was responsible for the change in seawater chemistry at Site U1356 during the EMET.

5.3.2. Changes in the Erosional Regime on Antarctica: Influence on Shallow Marine Records

The observed transient negative Nd isotope excursion in our fish tooth record at Site U1356 is also recorded on the Pacific side of the Tasman Gateway at Site 1171, but not at Site 1172. Two excursions in the fish tooth Nd isotopes at Site 1171 at ~48 and ~ 49 Ma are of a similar magnitude (~ 2 ε_{Nd}) to Site U1356 with respective $\varepsilon_{Nd(t)\ (MIN)}$ values of -12.4 at Site U1356 and -8.9 at Site 1171 at ~48 Ma (Figure 2) (note that there is uncertainty in the age of the excursion at Site 1171 (±0.5 Myr) due the low resolution of the age model; see supporting information for age model details). A similar additional excursion in seawater chemistry may have occurred at Site U1356. If it did, it was not recovered due to the hiatus between ~51 and ~49 Ma. Water mass mixing alone cannot be responsible for these observed excursions as no suitably unradiogenic water mass has been documented within the respective surrounding oceanic areas during the Eocene (Figure 6). However, Eocene bulk sediment Nd data at both sites are lower than the associated fish tooth records (U1356 sediment $\varepsilon_{Nd(t)} = -13.1$ to -14.7; 1171 sediment $\varepsilon_{Nd(t)} = -9.3$ to -9.8; Figure 3), reflecting the local bedrock composition around the areas of Wilkes Land, Adélie Coast and Northern Victoria Land (for a summary see *Pierce et al.* [2014]). We therefore conclude that changes in the erosional regime of the proximal geological source regions is likely to be responsible for the Nd isotope excursions detected at Sites U1356 and 1171. Relating the transient excursions in our fish tooth Nd records at Sites U1356 and 1171 to changing erosional fluxes from the Antarctic continent is also consistent with the absence of an excursion at Site 1172

between 48 and 49 Ma, as tectonic reconstructions place Site 1172 further north on the East Tasman Plateau [*Cande and Stock*, 2004; Figure 1].

We speculate that a period of intense erosion of the respective Antarctic source regions adjacent to Sites U1356 and 1171 (Figure 3) could have resulted in an increased flux of dissolved (and particulate) Nd to the shelf waters, modifying the composition of local waters toward the sedimentary Nd end-member. A similar mechanism was proposed by *Scher et al.* [2011] who suggested that the rapid growth and associated erosion of an ice sheet on Antarctica resulted in a pulse of unradiogenic Nd delivered to the Southern Ocean across the Eocene-Oligocene transition. Increased continental erosion may have occurred as a result of either higher precipitation levels or ephemeral glaciation in mountainous regions. Sediment Nd data alone cannot decipher which of these mechanisms was responsible for our records over the EMET. Our findings do, however, suggest that there may have been an important perturbation to the hydrological cycle on the Antarctic continent over this interval, which is expressed in the chemistry of the surrounding ocean.

5.3.3. Evidence for a Cooling Event During the EMET?

Constraining the erosional mechanism responsible for the Nd isotope excursion in our fish tooth records at Sites U1356 and 1171 relies on understanding the continental climate on Antarctica at the time. There is evidence for significant cooling during the EMET at both local and regional levels in the southern high latitudes, which may suggest that the development of small-scale highland ice sheets was a feasible driver for changing erosional conditions during the EMET. At Site U1356, bulk sediment geochemistry suggests a short-lived decrease in temperature and precipitation between 49 and 48 Ma [*Passchier et al.*, 2013] within same interval as the excursion in fish tooth Nd values. More regionally, a drop in deep water and sea surface temperatures at Site 277 and an increase in the deposition of siliciclastic sediments has also been reported from the mid-Waipara section in New Zealand at ~48.5 Ma [e.g., *Creech et al.*, 2010; *Hollis et al.*, 2009, 2012]. These regional responses to a transient cooling event on the Antarctic continent are superimposed on a prolonged environmental shift in the southern high latitudes from the early to middle Eocene. Fossil pollen extracted from Site U1356 sediments indicate a changing vegetation assemblage from high diversity plant ecosystems on the Antarctic continent during the early Eocene to a lower diversity, cooler assemblage in the middle Eocene [*Contreras et al.*, 2013; *Pross et al.*, 2012]. Similar terrestrial ecosystem changes have been reported from other sites around East Antarctica, the Antarctic Peninsula, and Southern Australia [e.g., *Askin*, 2000; *Francis et al.*, 2008; *Martin*, 2006; *Truswell and Macphail*, 2009].

Farther afield, the fish tooth Nd records from pelagic Sites 738 and 757 also reach minimum $\varepsilon_{Nd(t)}$ values during the EMET interval (Figure 2). The observation of a similar excursion in the fish tooth Nd record at Site 738 (located at ~62°S during the Eocene) to the shallow records from the Tasman Gateway implies that the proposed erosional event was widespread across East Antarctica. A similar record from Site 757 then further raises the question of whether the changes in Antarctic continental climate were propagated via intermediate/deep ocean currents to lower latitudes. If so, what was the associated impact? Increased Southern Ocean deep water export between 49 and 48 Ma has been inferred before in order to explain records of intensified bottom water currents and decreasing temperatures in the Atlantic and Pacific Ocean basins [e.g., *Barron et al.*, 2015; *Bralower et al.*, 1995; *Danelian et al.*, 2007; *Norris et al.*, 2001; *Ortiz and Thomas*, 2015; *Thomas et al.*, 2008]. The unradiogenic $\varepsilon_{Nd(t)}$ values between ~49 and 48 Ma at Sites 738 and 757 (Figure 5) may therefore be indicative of both an altered Nd isotopic composition of southern sourced seawater due to increased delivery of unradiogenic Nd to the surrounding continental shelves, as well as cooling in locations of deep water formation, resulting in invigorated propagation of Southern Ocean deep waters into the major ocean basins. Ultimately, to better understand the cause-or-consequence nature between Antarctic continental erosion, cooling over the EMET, and reinvigorated deep ocean circulation requires focused studies from cores with well-constrained age models across this little-studied, but pivotal, interval in Cenozoic climate history.

6. Conclusion

New Nd isotope data from fossil fish teeth and bulk sediments from pelagic and shallow marine settings in the Tasman region and surrounding areas of the Southern Ocean allow reconstruction of the distribution of intermediate/deep water masses during the early to middle Eocene. These data isotopically fingerprint the Antarctic shelves as the source of unradiogenic Nd isotope values that characterize the Indian Ocean

sector of the Southern Ocean and deep waters of the Indian Ocean during the Eocene. Additionally, we identify a new, locally formed intermediate-deep water mass in the Ross Sea region during the early to middle Eocene, but further research is required to conclude whether this unradiogenic deep water is exported from the SW Pacific or constitutes a specific layer in a stratified water column in the Ross Gyre. Finally, transient excursions in the fish tooth Nd isotope records at shallow marine sites U1356 and 1171 and pelagic, but proximal, Site 738 identify a period of increased flux of Nd from widespread locations on the Antarctic continent to the surrounding shelf seas. Results from Indian Ocean pelagic Site 757 furthermore suggest that this shelf water was then transported northward in intermediate/deep water masses. The increase in continental erosion on Antarctica potentially results from changes in the hydrological cycle in association with regional cooling documented at other regional and global locations between ~49 and 48 Ma during the EMET. Climatic changes on the Antarctic continent during the Eocene greenhouse may hence be communicated in deep waters across ocean basins, potentially influencing climate on a larger, global scale.

Acknowledgments
We gratefully acknowledge K. Kreissig and B. Coles for laboratory and technical support and Diederik Liebrand for many helpful discussions. We thank the Editor and reviewers for their constructive feedback, which has improved this manuscript. This research used samples and data provided by IODP. Funding for this research was provided by NERC grants awarded to T.v.d.F. (NE/L004607/1) and T.v.d.F. and S.M.B. (NE/I006257/1) and an ECORD Research Grant awarded to C.E.H. All data used for this study are available in the supporting information, cited references, and on the Pangaea database (www.pangaea.de). The authors declare no conflicting interests.

References

Anagnostou, E., E. H. John, K. M. Edgar, G. L. Foster, A. Ridgwell, G. N. Inglis, R. D. Pancost, D. J. Lunt, and P. N. Pearson (2016), Changing atmospheric CO_2 concentration was the primary driver of early Cenozoic climate, *Nature*, *533*(7603), 380–384.

Arsouze, T., J. Dutay, F. Lacan, and C. Jeandel (2009), Reconstructing the Nd oceanic cycle using a coupled dynamical-biogeochemical model, *Biogeosciences*, *6*(12), 2829–2846.

Askin, R. A. (2000), Spores and pollen from the McMurdo sound erratics, Antarctica, *Antarct. Res. Ser.*, *76*, 161–181.

Barron, J., et al. (1989), Proceedings of the Ocean Drilling Program: Initial Reports, vol. 119, 942 pp.

Barron, J. A., C. E. Stickley, and D. Bukry (2015), Paleoceanographic, and paleoclimatic constraints on the global Eocene diatom and silicoflagellate record, *Palaeogeogr. Palaeoclimatol. Palaeoecol.*, *422*, 85–100.

Bice, K. L., E. J. Barron, and W. H. Peterson (1997), Continental runoff and early Cenozoic bottom-water sources, *Geology*, *25*(10), 951–954.

Bijl, P. K., S. Schouten, A. Sluijs, G. J. Reichart, J. C. Zachos, and H. Brinkhuis (2009), Early Palaeogene temperature evolution of the southwest Pacific Ocean, *Nature*, *461*(7265), 776–779.

Bijl, P. K., A. Sluijs, and H. Brinkhuis (2013a), A magneto- and chemostratigraphically calibrated dinoflagellate cyst zonation of the early Paleogene South Pacific Ocean, *Earth Sci. Rev.*, *124*, 1–31.

Bijl, P. K., J. A. Bendle, S. M. Bohaty, J. Pross, S. Schouten, L. Tauxe, C. E. Stickley, R. M. McKay, U. Röhl, and M. Olney (2013b), Eocene cooling linked to early flow across the Tasmanian Gateway, *Proc. Natl. Acad. Sci. U.S.A.*, *110*(24), 9645–9650.

Boyle, E. A., and L. Keigwin (1985), Comparison of Atlantic and Pacific paleochemical records for the last 215, 000 years: Changes in deep ocean circulation and chemical inventories, *Earth Planet. Sci. Lett.*, *76*, 135–150.

Bohaty, S. M., and J. C. Zachos (2003), Significant Southern Ocean warming event in the late middle Eocene, *Geology*, *31*(11), 1017–1020.

Bohaty, S. M., J. C. Zachos, F. Florindo, and M. L. Delaney (2009), Coupled greenhouse warming and deep-sea acidification in the middle Eocene, *Paleoceanography*, *24*, PA2207, doi:10.1029/2008PA001676.

Borrelli, C., B. S. Cramer, and M. E. Katz (2014), Bipolar Atlantic deepwater circulation in the middle-late Eocene: Effects of Southern Ocean gateway openings, *Paleoceanography*, *29*, 308–327, doi:10.1002/2012PA002444.

Bralower, T. J., J. C. Zachos, E. Thomas, M. Parrow, C. K. Paull, D. C. Kelly, I. P. Silva, W. V. Sliter, and K. C. Lohmann (1995), Late Paleocene to Eocene paleoceanography of the equatorial Pacific Ocean: Stable isotopes recorded at ocean drilling program site 865, Allison Guyot, *Paleoceanography*, *10*, 841–865, doi:10.1029/95PA01143.

Brass, G. W., J. R. Southam, and W. H. Peterson (1982), Warm saline bottom water in the ancient ocean, *Nature*, *296*, 620–623.

Browning, J. V., K. G. Miller, and D. K. Pak (1996), Global implications of lower to middle Eocene sequence boundaries on the New Jersey coastal plain: The icehouse cometh, *Geology*, *24*(7), 639–642.

Burton, K. W., H. F. Ling, and R. K. O'Nions (1997), Closure of the Central American Isthmus and its effect on deep-water formation in the North Atlantic, *Nature*, *386*, 382–385.

Cande, S. C., and J. M. Stock (2004), Cenozoic reconstructions of the Australia-New Zealand-South Pacific sector of Antarctica, in *The Cenozoic Southern Ocean: Tectonics, Sedimentation, and Climate Change Between Australia and Antarctica*, edited by N. F. Exon, J. P. Kennett, and M. J. Malone, pp. 5–18, AGU, Washington, D. C.

Chavagnac, V., J. Milton, D. Green, J. Breuer, O. Bruguier, D. Jacob, T. Jong, G. Kamenov, J. Le Huray, and Y. Liu (2007), Towards the development of a fossil bone geochemical standard: An inter-laboratory study, *Anal. Chim. Acta*, *599*(2), 177–190.

Contreras, L., J. Pross, P. K. Bijl, A. Koutsodendris, J. I. Raine, B. van de Schootbrugge, and H. Brinkhuis (2013), Early to middle Eocene vegetation dynamics at the Wilkes Land Margin (Antarctica), *Rev. Palaeobot. Palynol.*, *197*, 119–142.

Cook, C. P., T. van de Flierdt, T. Williams, S. R. Hemming, M. Iwai, M. Kobayashi, F. J. Jimenez-Espejo, C. Escutia, J. J. González, and B.-K. Khim (2013), Dynamic behaviour of the East Antarctic ice sheet during Pliocene warmth, *Nat. Geosci.*, *6*(9), 765–769.

Corfield, R. M., and R. D. Norris (1996), Deep water circulation in the Paleocene ocean, in *Correlation of the Early Paleogene in North-West Europe*, edited by R. W. O'B. Knox, R. M. Corfield, and R. E. Dunay, *Geol. Soc. London Spec. Publ.*, vol. 101, pp. 443–456.

Coxall, H. K., P. A. Wilson, H. Palike, C. H. Lear, and J. Backman (2005), Rapid stepwise onset of Antarctic glaciation and deeper calcite compensation in the Pacific Ocean, *Nature*, *433*(7021), 53–57.

Cramer, B., J. Toggweiler, J. Wright, M. Katz, and K. Miller (2009), Ocean overturning since the Late Cretaceous: Inferences from a new benthic foraminiferal isotope compilation, *Paleoceanography*, *24*, PA4216, doi:10.1029/2008PA001683.

Creech, J. B., J. A. Baker, C. J. Hollis, H. E. Morgans, and E. G. Smith (2010), Eocene sea temperatures for the mid-latitude southwest Pacific from Mg/Ca ratios in planktonic and benthic foraminifera, *Earth Planet. Sci. Lett.*, *299*(3), 483–495.

Danelian, T., S. Saint Martin, and M.-M. Blanc-Valleron (2007), Middle Eocene radiolarian and diatom accumulation in the equatorial Atlantic (Demerara Rise, ODP Leg 207): Possible links with climatic and palaeoceanographic changes, *C. R. Palevol*, *6*(1–2), 103–114.

De Baar, H. J., M. P. Bacon, P. G. Brewer, and K. W. Bruland (1985), Rare earth elements in the Pacific and Atlantic Oceans, *Geochim. Cosmochim. Acta*, *49*(9), 1943–1959.

DeConto, R. M., and D. Pollard (2003), Rapid Cenozoic glaciation of Antarctica induced by declining atmospheric CO_2, *Nature*, *421*(6920), 245–249.

Douglas, P. M. J., H. P. Affek, L. C. Ivany, A. J. P. Houben, W. P. Sijp, A. Sluijs, S. Schouten, and M. Pagani (2014), Pronounced zonal heterogeneity in Eocene southern high-latitude sea surface temperatures, *Proc. Natl. Acad. Sci. U.S.A.*, *111*(18), 6582–6587.

Dunkley Jones, T., P. R. Bown, P. N. Pearson, B. S. Wade, H. K. Coxall, and C. H. Lear (2008), Major shifts in calcareous phytoplankton assemblages through the Eocene-Oligocene transition of Tanzania and their implications for low-latitude primary production, *Paleoceanography*, *23*, PA4204, doi:10.1029/2008PA001640.

Ehrmann, W. U., M. Melles, G. Kuhn, and H. Grobe (1992), Significance of clay mineral assemblages in the Antarctic Ocean, *Mar. Geol.*, *107*(4), 249–273.

Elderfield, H., and R. Pagett (1986), Rare earth elements in ichthyoliths: Variations with redox conditions and depositional environment, *Sci. Total Environ.*, *49*, 175–197.

Escutia, C., H. Brinkhius, A. Klaus, and the Expedition 318 Scientists (2011), Proceedings of the IODP, vol. 18.

Exon, N., J. P. Kennett, M. J. Malone, and the Expedition 189 Scientists (2001), The Tasmanian gateway: Cenozoic climatic and oceanographic development, Sites 1168-1172 Rep., Ocean Drilling Program.

Francis, J. E., et al. (2008), Chapter 8 from greenhouse to icehouse—The Eocene/Oligocene, in *Antarctica, in Developments in Earth and Environmental Sciences*, edited by F. Fabio, and S. Martin, pp. 309–368, Elsevier, Netherlands.

Freslon, N., G. Bayon, S. Toucanne, S. Bermell, C. Bollinger, S. Chéron, J. Etoubleau, Y. Germain, A. Khripounoff, and E. Ponzevera (2014), Rare earth elements and neodymium isotopes in sedimentary organic matter, *Geochim. Cosmochim. Acta*, *140*, 177–198.

Galeotti, S., et al. (2016), Antarctic Ice Sheet variability across the Eocene-Oligocene boundary climate transition, *Science*, *352*(6281), 76–80.

German, C. R., and H. Elderfield (1990), Application of the Ce anomaly as a paleoredox indicator: The ground rules, *Paleoceanography*, *5*, 823–833, doi:10.1029/PA005i005p00823.

Gingele, F., and P. De Deckker (2005), Clay mineral, geochemical and Sr–Nd isotopic fingerprinting of sediments in the Murray–Darling fluvial system, southeast Australia, *Aust. J. Earth Sci.*, *52*(6), 965–974.

Goldstein, S. J., and S. B. Jacobsen (1988), Nd and Sr isotopic systematics of river water suspended material: Implications for crustal evolution, *Earth Planet. Sci. Lett.*, *87*, 249–265.

Goldner, A., N. Herold, and M. Huber (2014), Antarctic glaciation caused ocean circulation changes at the Eocene-Oligocene transition, *Nature*, *511*, 574–577.

Hague, A. M., D. J. Thomas, M. Huber, R. Korty, S. C. Woodard, and L. B. Jones (2012), Convection of North Pacific deep water during the early Cenozoic, *Geology*, *40*(6), 527–530.

Hayes, D. E., et al. (1975), Initial reports of the Deep Sea Drilling Project, vol. 28, pp. 725–759, U.S. Gov. Print. Off., Washington, D. C.

Hohbein, M. W., P. F. Sexton, and J. A. Cartwright (2012), Onset of North Atlantic Deepwater production coincident with inception of the Cenozoic global cooling trend, *Geology*, *40*(3), 255–258.

Hollis, C. J., D. B. Waghorn, C. P. Strong, E. M. Crouch (1997), Integrated Paleogene biostratigraphy of DSDP site 277 (Leg 29): Foraminifera, calcareous nannofossils, Radiolaria, and palynomorphs, Institute of Geological and Nuclear Sciences Science Report, 97/07, 87 pp.

Hollis, C. J., L. Handley, E. M. Crouch, H. E. Morgans, J. A. Baker, J. Creech, K. S. Collins, S. J. Gibbs, M. Huber, and S. Schouten (2009), Tropical sea temperatures in the high-latitude South Pacific during the Eocene, *Geology*, *37*(2), 99–102.

Hollis, C. J., et al. (2012), Early Paleogene temperature history of the Southwest Pacific Ocean: Reconciling proxies and models, *Earth Planet. Sci. Lett.*, *349–350*, 53–66.

Hollis, C. J., B. R. Hines, K. Littler, V. Villasante-Marcos, D. K. Kulhanek, C. P. Strong, J. C. Zachos, S. M. Eggins, L. Northcote, and A. Phillips (2015), The Paleocene–Eocene Thermal Maximum at DSDP Site 277, Campbell Plateau, southern Pacific Ocean, *Clim. Past*, *11*(7), 1009–1025.

Houben, A. J. P., et al. (2013), Reorganization of Southern Ocean plankton ecosystem at the onset of Antarctic glaciation, *Science*, *340*(6130), 341–344.

Huber, M., and R. Caballero (2011), The early Eocene equable climate problem revisted, *Clim. Past*, *7*, 603–633.

Huber, M., and D. Nof (2006), The ocean circulation in the southern hemisphere and its climatic impacts in the Eocene, *Palaeogeogr. Palaeoclimatol. Palaeoecol.*, *231*(1), 9–28.

Huber, M., and L. C. Sloan (2001), Heat transport, deep waters, and thermal gradients: Coupled simulation of an Eocene greenhouse climate, *Geophys. Res. Lett.*, *28*, 3481–3484, doi:10.1029/2001GL012943.

Huber, B. T., and F. Quillévéré (2005), Revised Paleogene planktonic foraminiferal biozonation for the Austral realm, *J. Foraminifer. Res.*, *35*(4), 299–314.

Huber, M., H. Brinkhuis, C. E. Stickley, K. Döös, A. Sluijs, J. Warnaar, S. A. Schellenberg, and G. L. Williams (2004), Eocene circulation of the Southern Ocean: Was Antarctica kept warm by subtropical waters?, *Paleoceanography*, *19*, PA4026, doi:10.1029/2004PA001014.

Huck, C. E., T. van de Flierdt, F. J. Jiménez-Espejo, S. M. Bohaty, U. Röhl, and S. J. Hammond (2016), Robustness of fossil fish teeth for seawater neodymium isotope reconstructions under variable redox conditions in an ancient shallow marine setting, *Geochem. Geophys. Geosyst.*, *17*, 679–698, doi:10.1002/2015GC006218.

Jacobsen, S. B., and G. Wasserburg (1980), Sm-Nd isotopic evolution of chondrites, *Earth Planet. Sci. Lett.*, *50*(1), 139–155.

Jeandel, C., T. Arsouze, F. Lacan, P. Téchiné, and J.-C. Dutay (2007), Isotopic Nd compositions and concentrations of the lithogenic inputs into the ocean: A compilation, with an emphasis on the margins, *Chem. Geol.*, *239*, 156–164.

Jovane, L., R. Coccioni, A. Marsili and G. Acton (2009), The late Eocene greenhouse–icehouse transition: Observations from the Massignano global stratotype section and point (GSSP), in *The Late Eocene Earth—Hothouse, Ice-House, and Impacts*, edited by C. Koeberl and A. Montanari, *Geol. Soc. Am. Spec. Pap.*, 452, pp. 149–168.

Katz, M. E., B. S. Cramer, J. Toggweiler, G. Esmay, C. Liu, K. G. Miller, Y. Rosenthal, B. S. Wade, and J. D. Wright (2011), Impact of Antarctic Circumpolar current development on late Paleogene ocean structure, *Science*, *332*(6033), 1076–1079.

Kennett, J. P. (1977), Cenozoic evolution of Antarctic glaciation, the Circum-Antarctic Ocean, and their impact on global paleoceanography, *J. Geophys. Res.*, *82*, 3843–3860, doi:10.1029/JC082i027p03843.

Kennett, J. P., et al. (1975), Initial reports of the Deep Sea Drilling project, vol. 29, 1186 pp.

Kennett, J. P., and L. D. Stott (1991), Abrupt deep sea warming, paleoceanographic changes and benthic extinctions at the end of the Paleocene, *Nature*, *353*, 319–322.

Kent, D. V., and G. Muttoni (2008), Equatorial convergence of India and early Cenozoic climate trends, *Proc. Natl. Acad. Sci. U.S.A.*, *105*(42), 16,065–16,070.

Kent, D. V., and G. Muttoni (2013), Modulation of Late Cretaceous and Cenozoic climate by variable drawdown of atmospheric pCO_2 from weathering of basaltic provinces on continents drifting through the equatorial humid belt, *Clim. Past*, *9*(2), 525–546.

Kominz, M., J. Browning, K. Miller, P. Sugarman, S. Mizintseva, and C. Scotese (2008), Late Cretaceous to Miocene sea-level estimates from the New Jersey and Delaware coastal plain coreholes: An error analysis, *Basin Res.*, *20*(2), 211–226.

Lambelet, M., T. van de Flierdt, E. C. V. Butler, A. R. Bowie, S. R. Rintoul, R. J. Watson, T. Remenyl, and D. Lannuzel (2014), The Nd isotopic compositions of Adélie coast bottom water—Insights from GIPY6 cruise along 140′, Abstract OS21G-07 presented at 2014 Fall Meeting 2014, AGU, San Francisco, Calif.

Lawver, L. A., and L. M. Gahagan (2003), Evolution of Cenozoic seaways in the circum-Antarctic region, *Palaeogeogr. Palaeoclimatol. Palaeoecol.*, *198*(1), 11–37.

Le Houedec, S., L. Meynadier, and C. J. Allègre (2016), Seawater Nd isotope variation in the Western Pacific Ocean since 80 Ma (ODP 807, Ontong Java Plateau), *Mar. Geol.*, *380*, 138–147.

Lear, C. H., T. R. Bailey, P. N. Pearson, H. K. Coxall, and Y. Rosenthal (2008), Cooling and ice growth across the Eocene-Oligocene transition, *Geology*, *36*(3), 251–254.

Ling, H. F., K. W. Burton, R. K. O'Nions, B. S. Kamber, F. von Blanckenburg, A. J. Gibb, and J. R. Hein (1997), Evolution of Nd and Pb isotopes in Central Pacific seawater from ferromanganese crusts, *Earth Planet. Sci. Lett.*, *146*(1–2), 1–12.

Ling, H. F., S.-Y. Jiang, M. Frank, H.-Y. Zhou, F. Zhou, Z.-L. Lu, X.-M. Chen, Y.-H. Jiang, and C.-D. Ge (2005), Differing controls over the Cenozoic Pb and Nd isotope evolution of deepwater in the central North Pacific Ocean, *Earth Planet. Sci. Lett.*, *232*, 345–361.

Littler, K., U. Röhl, T. Westerhold, and J. C. Zachos (2014), A high-resolution benthic stable-isotope record for the South Atlantic: Implications for orbital-scale changes in Late Paleocene–early Eocene climate and carbon cycling, *Earth Planet. Sci. Lett.*, *401*, 18–30.

Liu, Z. H., M. Pagani, D. Zinniker, R. DeConto, M. Huber, H. Brinkhuis, S. R. Shah, R. M. Leckie, and A. Pearson (2009), Global cooling during the Eocene-Oligocene climate transition, *Science*, *323*(5918), 1187–1190.

Lunt, D. J., P. J. Valdes, T. Dunkley-Jones, A. Ridgwell, A. M. Haywood, D. N. Schmidt, R. Marsh, and M. Maslin (2010), CO_2-driven ocean circulation changes as an amplifier of Paleocene-Eocene thermal maximum hydrate destabilization, *Geology*, *38*(10), 875–878.

MacLeod, K. G., C. Isaza-Londoño, E. E. Martin, A. Jimenez Berrocoso, C. Basak (2011), Changes in North Atlantic circulation at the end of the Cretaceous greenhouse interval, *Nat. Geosci.*, *4*, 779–782.

Martin, E. E., and B. A. Haley (2000), Fossil fish teeth as proxies for seawater Sr and Nd isotopes, *Geochim. Cosmochim. Acta*, *64*(5), 835–847.

Martin, E. E., and H. Scher (2006), A Nd isotopic study of southern sourced waters and Indonesian throughflow at intermediate depths in the Cenozoic Indian Ocean, *Geochem. Geophys. Geosyst.*, *7*, Q09N02, doi:10.1029/2006GC001302.

Martin, E., K. Macleod, A. Jiménez Berrocoso and E. Bourbon (2012), Water mass circulation on Demerara Rise during the Late Cretaceous based on Nd isotopes, *Earth Planet. Sci. Lett.*, *327*, 111–120.

Martin, H. (2006), Cenozoic climatic change and the development of the arid vegetation in Australia, *J. Arid Environ.*, *66*(3), 533–563.

McIntosh, W. C. (2000), $^{40}Ar/^{39}Ar$ geochronology of tephra and volcanic clasts in CRP-2A, Victoria Land Basin, Antarctica, *Terra Antarct.*, *7*, 621–630.

Miller, K. G., R. G. Fairbanks, and G. S. Mountain (1987), Tertiary oxygen isotope synthesis, sea level history, and continental margin erosion, *Paleoceanography*, *2*, 1–19, doi:10.1029/PA002i001p00001.

Moiroud, M., E. Pucéat, Y. Donnadieu, G. Bayon, K. Moriya, J.-F. Deconinck, and M. Boyet (2013), Evolution of the neodymium isotopic signature of neritic seawater on a northwestern Pacific margin: New constrains on possible end-members for the composition of deep-water masses in the Late Cretaceous ocean, *Chem. Geol.*, *356*, 160–170.

Norris, R. D., A. Klaus, and D. Kroon (2001), Mid-Eocene deep water, the Late Palaeocene thermal maximum and continental slope mass wasting during the Cretaceous-Palaeogene impact, *Geol. Soc. London Spec. Publ.*, *183*(1), 23–48.

O'Nions, R. K., M. Frank, F. von Blanckenburg and H. F. Ling (1998), Secular variation of Nd and Pb isotopes in ferromanganese crusts from the At- lantic, Indian and Pacific Oceans, Earth Planet. *Sci. Lett.*, *155*, 15–28.

Orsi, A. H., and C. L. Wiederwohl (2009), A recount of Ross Sea waters, *Deep Sea Res., Part II*, *56*(13), 778–795.

Ortiz, S., and E. Thomas (2015), Deep-sea benthic foraminiferal turnover during the early–middle Eocene transition at Walvis Ridge (SE Atlantic), *Palaeogeogr. Palaeoclimatol. Palaeoecol.*, *417*, 126–136.

Otto-Bliesner, B. L., E. C. Brady, and C. Shields (2002), Late Cretaceous ocean: Coupled simulations with the National Center for Atmospheric Research Climate System Model, *J. Geophys. Res.*, *107*(D2), 4019, doi:10.1029/2001JD000821.

Pagani, M., J. C. Zachos, K. H. Freeman, B. Tipple, and S. Bohaty (2005), Marked decline in atmospheric carbon dioxide concentrations during the Paleogene, *Science*, *309*(5734), 600–603.

Pagani, M., M. Huber, Z. Liu, S. M. Bohaty, J. Henderiks, W. Sijp, S. Krishnan, and R. M. DeConto (2011), The role of carbon dioxide during the onset of Antarctic glaciation, *Science*, *334*(6060), 1261–1264.

Pak, D. K., and K. G. Miller (1992), Paleocene to Eocene benthic foraminiferal isotopes and assemblages: Implications for deepwater circulation, *Paleoceanography*, *7*, 405–422, doi:10.1029/92PA01234.

Pankhurst, R. J., S. D. Weaver, J. D. Bradshaw, B. C. Storey, and T. R. Ireland (1998), Geochronology and geochemistry of pre-Jurassic superterranes in Marie Byrd Land, Antarctica, *J. Geophys. Res.*, *103*, 2529–2547, doi:10.1029/97JB02605.

Passchier, S., S. M. Bohaty, F. Jiménez-Espejo, J. Pross, U. Röhl, T. van de Flierdt, C. Escutia, and H. Brinkhuis (2013), Early Eocene to middle Miocene cooling and aridification of East Antarctica, *Geochem. Geophys. Geosyst.*, *14*, 1399–1410, doi:10.1002/ggge.20106.

Passchier, S., D. J. Ciarletta, T. E. Miriagos, P. K. Bijl, and S. M. Bohaty (2017), An Antarctic stratigraphic record of stepwise ice growth through the Eocene-Oligocene transition, *Geol. Soc. Am. Bull.*, *29*(3/4), 318–330.

Peirce, J., et al. (1989), *Proceedings of the Ocean Drilling Project: Initial Reports*, vol. 121, pp. 359–453, Ocean Drilling Program, College Station, Tex.

Pekar, S. F., A. Hucks, M. Fuller, and S. Li (2005), Glacioeustatic changes in the early and middle Eocene (51–42 Ma): Shallow-water stratigraphy from ODP Leg 189 Site 1171 (South Tasman Rise) and deep-sea δ18O records, *Geol. Soc. Am. Bull.*, *117*(7–8), 1081–1093.

Pucéat, E., C. Lécuyer, and L. Reisberg (2005), Neodymium isotope evolution of NW Tethyan upper ocean waters throughout the Cretaceous, *Earth Planet. Sci. Lett.*, *236*, 705–720.

Pierce, E., S. Hemming, T. Williams, T. van de Flierdt, S. Thomson, P. Reiners, G. Gehrels, S. Brachfeld, and S. Goldstein (2014), A comparison of detrital U–Pb zircon, 40 Ar/39 Ar hornblende, 40 Ar/39 Ar biotite ages in marine sediments off East Antarctica: Implications for the geology of subglacial terrains and provenance studies, *Earth Sci. Rev.*, *138*, 156–178.

Pierce, E. L., T. Williams, T. Flierdt, S. R. Hemming, S. L. Goldstein, and S. A. Brachfeld (2011), Characterizing the sediment provenance of East Antarctica's weak underbelly: The Aurora and Wilkes sub-glacial basins, *Paleoceanography*, *26*, PA4217, doi:10.1029/2011PA002127.

Pin, C., and J. S. Zalduegui (1997), Sequential separation of light rare-earth elements, thorium and uranium by miniaturized extraction chromatography: Application to isotopic analyses of silicate rocks, *Anal. Chim. Acta*, *339*(1), 79–89.

Poulsen, C. J., E. J. Barron, C. C. Johnson, and P. Fawcett (1999), Links between major climatic factors and regional oceanic circulation in the mid-Cretaceous, *Geol. Soc. Am. Spec. Pap.*, 73–90.

Pross, J., L. Contreras, P. K. Bijl, D. R. Greenwood, S. M. Bohaty, S. Schouten, J. A. Bendle, U. Röhl, L. Tauxe, and J. I. Raine (2012), Persistent near-tropical warmth on the Antarctic continent during the early Eocene epoch, *Nature*, *488*(7409), 73–77.

Rickli, J., M. Gutjahr, D. Vance, M. Fischer-Gödde, C.-D. Hillenbrand, and G. Kuhn (2014), Neodymium and hafnium boundary contributions to seawater along the West Antarctic continental margin, *Earth Planet. Sci. Lett.*, *394*, 99–110.

Roberts, A. P., F. Florindo, G. Villa, L. Chang, L. Jovane, S. M. Bohaty, J. C. Larrasoaña, D. Heslop, and J. D. Fitz Gerald (2011), Magnetotactic bacterial abundance in pelagic marine environments is limited by organic carbon flux and availability of dissolved iron, *Earth Planet. Sci. Lett.*, *310*, 441–452.

Roberts, A. P., L. Sagnotti, F. Florindo, S. M. Bohaty, K. L. Verosub, G. S. Wilson, and J. C. Zachos (2013), Environmental record of paleoclimate, unroofing of the Transantarctic Mountains, and volcanism in later Eocene to early Miocene glaci-marine sediments from the Victoria Land Basin, Ross Sea, Antarctica, *J. Geophys. Res. Solid Earth*, *118*, 1845–1861, doi:10.1002/jgrb.50151.

Robinson, S. A., D. P. Murphy, D. Vance, and D. J. Thomas (2010), Formation of "Southern Component Water" in the Late Cretaceous: Evidence from Nd-isotopes, *Geology*, *38*, 871–874.

Scher, H. D., and E. E. Martin (2004), Circulation in the Southern Ocean during the Paleogene inferred from neodymium isotopes, *Earth Planet. Sci. Lett.*, *228*(3–4), 391–405.

Scher, H. D., and E. E. Martin (2006), Timing and climatic consequences of the opening of Drake Passage, *Science*, *312*(5772), 428–430.

Scher, H. D., and E. E. Martin (2008), Oligocene deep water export from the North Atlantic and the development of the Antarctic Circumpolar Current examined with neodymium isotopes, *Paleoceanography*, *23*, PA1205, doi:10.1029/2006PA001400.

Scher, H. D., and M. L. Delaney (2010), Breaking the glass ceiling for high resolution Nd isotope records in early Cenozoic paleoceanography, *Chem. Geol.*, *269*(3), 329–338.

Scher, H. D., S. M. Bohaty, J. C. Zachos, and M. L. Delaney (2011), Two-stepping into the icehouse: East Antarctic weathering during progressive ice-sheet expansion at the Eocene–Oligocene transition, *Geology*, *39*(4), 383–386.

Scher, H. D., S. M. Bohaty, B. W. Smith, and G. H. Munn (2014), Isotopic interrogation of a suspected late Eocene glaciation, *Paleoceanography*, *29*, 628–644, doi:10.1002/2014PA002648.

Scher, H. D., J. M. Whittaker, S. E. Williams, J. C. Latimer, W. E. Kordesch, and M. L. Delaney (2015), Onset of Antarctic Circumpolar Current 30 million years ago as Tasmanian Gateway aligned with westerlies, *Nature*, *523*(7562), 580–583.

Sexton, P. F., P. A. Wilson, and R. D. Norris (2006), Testing the Cenozoic multisite composite δ18O and δ13C curves: New monospecific Eocene records from a single locality, Demerara Rise (Ocean Drilling Program Leg 207), *Paleoceanography*, *21*, PA2019, doi:10.1029/2005PA001253.

Sexton, P. F., R. D. Norris, P. A. Wilson, H. Pälike, T. Westerhold, U. Röhl, C. T. Bolton, and S. Gibbs (2011), Eocene global warming events driven by ventilation of oceanic dissolved organic carbon, *Nature*, *471*(7338), 349–352.

Shaw, H., and G. Wasserburg (1985), Sm-Nd in marine carbonates and phosphates: Implications for Nd isotopes in seawater and crustal ages, *Geochim. Cosmochim. Acta*, *49*(2), 503–518.

Sijp, W. P., and M. H. England (2016), The effect of low ancient greenhouse temperature gradients on the ocean's overturning circulation, *Clim. Past*, *12*, 543–552.

Sijp, W. P., M. H. England, and M. Huber (2011), Effect of the deepening of the Tasman Gateway on the global ocean, *Paleoceanography*, *26*, PA4207, doi:10.1029/2011PA002143.

Soudry, D., C. R. Glenn, Y. Nathan, I. Segal, and D. Vonder Haar (2006), Evolution of Tethyan phosphogenesis along the northern edges of the Arabian-African shield during the Cretaceous-Eocene as deduced from temporal variations of Ca and Nd isotopes and rates of P accumulation, *Earth Sci. Rev.*, *78*, 27–57.

Stichel, T., M. Frank, J. Rickli, and B. A. Haley (2012), The hafnium and neodymium isotope composition of seawater in the Atlantic sector of the Southern Ocean, *Earth Planet. Sci. Lett.*, *317*, 282–294.

Stille, P., and H. Fischer (1990), Secular variation in the isotopic composition of Nd in Tethys seawater, *Geochim. Cosmochim. Acta*, *54*, 3139–3145.

Tachikawa, K., V. Athias, and C. Jeandel (2003), Neodymium budget in the modern ocean and paleo-oceanographic implications, *J. Geophys. Res.*, *108*(8), 3254, doi:10.1029/1999JC000285.

Tanaka, T., et al. (2000), JNdi-1: A neodymium isotopic reference in consistency with LaJolla neodymium, *Chem. Geol.*, *168*, 279–281.

Tauxe, L., C. Stickley, S. Sugisaki, P. Bijl, S. Bohaty, H. Brinkhuis, C. Escutia, J. Flores, A. Houben, and M. Iwai (2012), Chronostratigraphic framework for the IODP Expedition 318 cores from the Wilkes Land Margin: Constraints for paleoceanographic reconstruction, *Paleoceanography*, *27*, PA2214, doi:10.1029/2012PA002308.

Taylor, S. R., and S. M. McLennan (1985), *The Continental Crust: Its Composition and Evolution*, 312 pp., Blackwell Scientific Publ., Oxford, U. K.

Thomas, D. J. (2004), Evidence for deep-water production in the North Pacific Ocean during the early Cenozoic warm interval, *Nature*, *430*(6995), 65–68.

Thomas, D. J., T. J. Bralower, and C. E. Jones (2003), Neodymium isotopic reconstruction of late Paleocene-early Eocene thermohaline circulation, *Earth Planet. Sci. Lett.*, *209*(3–4), 309–322.

Thomas, D. J., M. Lyle, T. C. Moore, and D. K. Rea (2008), Paleogene deepwater mass composition of the tropical Pacific and implications for thermohaline circulation in a greenhouse world, *Geochem. Geophys. Geosyst.*, *9*, Q02002, doi:10.1029/2007GC001748.

Thomas, D. J., R. Korty, M. Huber, J. A. Schubert, and B. Haines (2014), Nd isotopic structure of the Pacific Ocean 70–30 Ma and numerical evidence for vigorous ocean circulation and ocean heat transport in a greenhouse world, *Paleoceanography*, *29*, 454–469, doi:10.1002/2013PA002535.

Truswell, E. M., and M. K. Macphail (2009), Polar forests on the edge of extinction: What does the fossil spore and pollen evidence from East Antarctica say?, *Aust. Syst. Bot.*, *22*(2), 57–106.

Uenzelmann-Neben, G., T. Weber, J. Grützner, and M. Thomas (2016), Transition from the Cretaceous ocean to Cenozoic circulation in the western South Atlantic—A twofold reconstruction, *Tectonophysics*, doi:10.1016/j.tecto.2016.05.036.

van de Flierdt, T., S. R. Hemming, S. L. Goldstein, and W. Abouchami (2006), Radiogenic isotope fingerprint of Wilkes Land–Adélie coast bottom water in the circum-Antarctic Ocean, *Geophys. Res. Lett.*, *33*, L12606, doi:10.1029/2006GL026020.

van de Flierdt, T., M. Frank, A. N. Halliday, J. R. Hein, B. Hattendorf, D. Günther, and P. W. Kubik (2004), Deep and bottom water export from the Southern Ocean to the Pacific over the past 38 million years, *Paleoceanography*, *19*, PA1020, doi:10.1029/2003PA000923.

van Hinsbergen, D. J., L. V. de Groot, S. J. van Schaik, W. Spakman, P. K. Bijl, A. Sluijs, C. G. Langereis, and H. Brinkhuis (2015), A paleolatitude calculator for paleoclimate studies, *PLoS One*, *10*(6), e0126946.

Vandenberghe, N., R. P. Speijer, and F. J. Hilgen (2012), The Paleogene period, in *The Geologic Time Scale 2012*, edited by F. M. Gradstein et al., pp. 855–922, Elsevier, Amsterdam.

Via, R. K., and D. J. Thomas (2006), Evolution of Atlantic thermohaline circulation: Early Oligocene onset of deep-water production in the North Atlantic, *Geology*, *34*(6), 441–444.

Weis, D., et al. (2006), High-precision isotopic characterization of USGS reference materials by TIMS and MC-ICP-MS, *Geochem. Geophys. Geosyst.*, *7*, Q08006, doi:10.1029/2006GC001283.

Wright, J., H. Schrader, and W. T. Holser (1987), Paleoredox variations in ancient oceans recorded by rare earth elements in fossil apatite, *Geochim. Cosmochim. Acta*, *51*(3), 631–644.

Zachos, J., D. Rea, K. Seto, N. Niitsuma, and R. Nomura (1992), Paleogene and early Neogene deep water history of the Indian Ocean: Inferences from stable isotopic records, in *The Indian Ocean: A Synthesis of Results from the Ocean Drilling Program*, *Geophys. Monogr.*, vol. 70, pp. 351–386, AGU, Washington, D. C.

Zachos, J., M. Pagani, L. Sloan, E. Thomas, and K. Billups (2001), Trends, rhythms, and aberrations in global climate 65 Ma to present, *Science*, *292*(5517), 686–693.

Zachos, J. C., L. D. Stott, and K. C. Lohmann (1994), Evolution of early Cenozoic marine temperatures, *Paleoceanography*, *9*, 353–387, doi:10.1029/93PA03266.

Zachos, J. C., G. R. Dickens, and R. E. Zeebe (2008), An early Cenozoic perspective on greenhouse warming and carbon-cycle dynamics, *Nature*, *451*(7176), 279–283.